arXiv:2302.01463v1 [cs.LG] 2 Feb 2023

Convergence of Gradient Descent with Linearly Correlated Noise and Applications to Differentially Private Learning

Anastasia Koloskova [*1] **Ryan McKenna** [2] **Zachary Charles** [2] **Keith Rush** [2] **Brendan McMahan** [2]

Abstract

We study stochastic optimization with linearly correlated noise. Our study is motivated by recent methods for optimization with differential privacy (DP), such as DP-FTRL, which inject noise via matrix factorization mechanisms. We propose an optimization problem that distils key facets of these DP methods and that involves perturbing gradients by linearly correlated noise. We derive improved convergence rates for gradient descent in this framework for convex and non-convex loss functions. Our theoretical analysis is novel and might be of independent interest. We use these convergence rates to develop new, effective matrix factorizations for differentially private optimization, and highlight the benefits of these factorizations theoretically and empirically.

1. Introduction

Differential privacy (DP) is a critical framework for designing algorithms with provable statistical privacy guarantees. Differentially private stochastic gradient descent (DP-SGD, Abadi et al. (2016)) is particularly important for enabling differentially private optimization of machine learning models. Many works have analyzed the convergence behavior of differentially private empirical risk minimization methods, including DP-SGD (Bassily et al., 2019; Feldman et al., 2022; Wang et al., 2017; Das et al., 2022). However, obtaining good privacy/utility trade-offs using DP-SGD with uncorrelated per-iterate noise can crucially require excessively large batch sizes or privacy amplification techniques such as subsampling (Bassily et al., 2014; 2019; Zhu & Wang, 2019) and shuffling (Erlingsson et al., 2019; Feldman et al., 2022). In some applications, including cross-device federated learning, limited and device-controlled client availability can make sampling or shuffling infeasible (Kairouz et al., 2021b). Even in centralized learning, many implementations of DP-SGD do not properly use the Poisson subsampling scheme in Abadi et al. (2016) for amplification, and instead use a single fixed shuffle of the dataset (Choquette-Choo et al., 2022).

Recent work by Kairouz et al. (2021a) provides an alternative method, DP-FTRL, which can attain good privacy/utility trade-offs without amplification. Their key insight is that for SGD-style algorithms, the error on *prefix sums* of gradients is more important than the error on individual gradients. By adding carefully correlated noise to the gradients, one can reduce the error on the prefix sums, at the cost of increased error on the individual gradients under a fixed privacy budget. The DP-FTRL mechanism is competitive or better than DP-SGD, even without relying on privacy amplification. In follow-up work, Denisov et al. (2022); Choquette-Choo et al. (2022) develop a refinement of DP-FTRL, MF-DP-FTRL, by formulating and solving a problem to find the "optimal" correlated noise structure under DP constraints. However, their notion of optimality is based on the expected total squared error of prefix sums of gradients. While this quantity can be related to a convergence bound, this bound can be loose. This raises questions about whether there are notions of optimality that better capture convergence behavior of such algorithms with correlated noise.

In this paper we study this class of mechanisms more closely and provide a detailed analysis of linearly correlated noise from an optimization point of view.

Our main contributions are summarized as follows:

- We propose a novel stochastic optimization problem that extracts key facets of methods like (MF-)DP-FTRL, and which isolates the effects of linearly correlated noise on optimization.
- We derive convergence rates for gradient descent in such settings that showcase the effect of linearly correlated noise and recover tight convergence rates in notable special cases. We use a novel proof technique that may be of independent interest.
- We use this theory to design a new mechanism within the MF-DP-FTRL framework with improved convergence properties. We demonstrate the effectiveness of

[*]Work performed while doing an internship at Google Research. [1]EPFL, Switzerland [2]Google Research. Correspondence to: Anastasia Koloskova <anastasia.koloskova@epfl.ch>, Ryan McKenna <mckennar@google.com>.

this mechanism empirically on a variety of datasets and tasks, matching or outperforming prior methods.

1.1. Related Work

Matrix mechanisms for differential privacy. Our work is inspired by recent progress on differentially private optimization using matrix mechanisms (Li et al., 2015). Historically, such mechanisms were mainly applied to linear statistical queries (Li et al., 2010; McKenna et al., 2018; Edmonds et al., 2020; Henzinger & Upadhyay, 2022). Denisov et al. (2022) and Choquette-Choo et al. (2022) extended these mechanisms to the adaptive streaming setting, allowing their application to optimization with DP. Denisov et al. (2022) show that this framework (MF-DP-FTRL) subsumes and improves the DP-FTRL algorithm (Kairouz et al., 2021a). Both DP-FTRL and MF-DP-FTRL improve privacy guarantees relative to DP-SGD (Abadi et al., 2016) without amplification. Our work studies the relationship between the correlated noise introduced by matrix factorization and the downstream effect on learning performance.

SGD with correlated noise. Stochastic noise in optimization arises in a variety of ways, including minibatching (Dekel et al., 2012) and explicit noise injection (Duchi et al., 2012; Zhou et al., 2019; Jin et al., 2021). While most analyses of SGD assume this noise is independent across iterates, some work considers correlated noise. For example, shuffle SGD involves correlated noise due to sampling without replacement (Mishchenko et al., 2020; Yun et al., 2022). Chen et al. (2020) analyze SGD when the noise comes from a Gaussian process that injects correlated noise. Lucchi et al. (2022) use correlated Brownian motion to improve SGD's ability to explore the loss landscape. Recently, Orvieto et al. (2022a;b) investigated anti-correlated noise as a way to impose regularization and improve generalization. In our work, we consider a linearly correlated noise model, and analyze its impact on SGD's convergence to critical points.

SGD with biased noise. Many algorithms can be viewed as SGD with structured but potentially biased noise, including SGD with (biased) compression (Stich et al., 2018; Gorbunov et al., 2020), delayed SGD (Mania et al., 2017; Dutta et al., 2018), local SGD (Stich, 2019), federated learning methods (Karimireddy et al., 2020; Yuan & Ma, 2020; Mitra et al., 2021; Nguyen et al., 2022), decentralized optimization methods (Yu et al., 2019; Koloskova et al., 2020), and many others. Convergence analyses for such methods often use techniques like perturbed iterate analysis (Mania et al., 2017). However, as we show in Section 4, directly applying such techniques to linearly correlated noise does not lead to tight convergence guarantees.

2. Background

In this work, we focus on an empirical risk minimization problem of the form

$$\min_{\mathbf{x}\in\mathbb{R}^d}\left[f(\mathbf{x}) = \frac{1}{n}\sum_{i=1}^{n} l(\mathbf{x},\xi_i)\right], \tag{1}$$

where $l(\mathbf{x},\xi_i)$ is the loss of the model $\mathbf{x}$ on the data point ξ_i, and n is the training set size. We would like to solve (1) while guaranteeing a notion of privacy for the training set $\{\xi_1,\dots,\xi_n\}$. One particular notion of privacy, *differential privacy* (DP, Dwork et al. (2006)), has emerged in recent years as the gold standard for anonymous data release. DP guarantees statistical difficulty in distinguishing whether or not a particular unit's data served as an input to a given algorithm, based on the algorithm's output. This protected unit may represent a single training example or a semantically higher-level unit like the entirety of a user's data.

While there are many optimization methods for solving (1), we will follow Denisov et al. (2022); Choquette-Choo et al. (2022) and restrict to first-order algorithms $\mathfrak{A}$ that combine previous (stochastic) gradients $\mathbf{g}_t$ in a linear manner. Each algorithm $\mathcal{A}\in\mathfrak{A}$ is parameterized by 1) a learning rate $\gamma>0$ and 2) scalars $\{a_{tj}\}_{1\le j\le t}$. These scalars are chosen a priori and do not change at runtime. Given a starting point $\mathbf{x}_0$, $\mathcal{A}$ produces iterates $\mathbf{x}_t\in\mathbb{R}^d$ given by:

$$\mathbf{x}_{t+1} = \mathbf{x}_0 - \gamma\mathcal{A}_t(\mathbf{g}_1,\dots,\mathbf{g}_t)$$
$$\mathcal{A}_t(\mathbf{g}_1,\dots,\mathbf{g}_t) = \sum_{j=1}^{t} a_{tj}\mathbf{g}_j,$$

where $\mathbf{g}_t$ is a (stochastic) gradient of f computed at $\mathbf{x}_t$.

This formulation encompasses many important first-order algorithms, including SGD (Robbins & Monro, 1951), SGD with momentum (Polyak, 1964; Nesterov, 1983), and delayed SGD (Agarwal & Duchi, 2011). This class also captures algorithms that use learning rate scheduling, so long as the schedule is independent of the gradient values.

We note for posterity that in the *single-epoch* setting analyzed by Denisov et al. (2022), these gradients have a specific structure. Namely, we fix a permutation of the training set $\{\zeta_1,\dots,\zeta_n\}$ and form T mini-batches $B_1,\dots,B_T$ sequentially from this shuffled dataset. The stochastic gradients are then formed via $\mathbf{g}_t = |B_t|^{-1}\sum_{i\in B_t}\nabla f(\mathbf{x}_t,\zeta_i)$.

It will be convenient to re-write the output of $\mathcal{A}$ in matrix notation. Fix a number of iterations T. We define

$$\mathbf{X} = [\mathbf{x}_1,\dots,\mathbf{x}_T]^\top\in\mathbb{R}^{T\times d},\ \mathbf{X}_0 = [\mathbf{x}_0,\dots,\mathbf{x}_0]^\top\in\mathbb{R}^{T\times d}$$
$$\mathbf{G} = [\mathbf{g}_1,\dots,\mathbf{g}_T]^\top\in\mathbb{R}^{T\times d},\ \mathbf{A} = [a_{ij}]_{1\le i,j\le T}\in\mathbb{R}^{T\times T}$$

Since the algorithm can combine only previously computed

gradients $\mathbf{g}_j$, we assume $a_{tj} = 0$ for $j > t$, so $\mathbf{A}$ is lower-triangular. In this notation, the iterates of $\mathcal{A}$ can be written:

$$\mathbf{X} = \mathbf{X}_0 - \gamma \mathbf{A}\mathbf{G}. \tag{2}$$

Example 2.1 (SGD)**.** Define the *prefix-sum* matrix $\mathbf{S} \in \mathbb{R}^{T\times T}$ as the lower-triangular matrix whose lower triangle is all ones. If $\mathbf{A} = \mathbf{S}$, then (2) is simply SGD with learning rate γ. As discussed by Denisov et al. (2022, Section 4), we also recover SGD with momentum using an appropriate transformation $\mathbf{S}'$ of $\mathbf{S}$.

2.1. Matrix Factorization and Privacy Mechanisms

In order to make the output of (2) differentially private, we typically need to clip the gradients $\mathbf{G}$ and add noise. Let $\overline{\mathbf{G}}$ denote the matrix whose rows (gradients) have been clipped to some ℓ_2 threshold α. Let $\mathbf{Z} \in \mathbb{R}^{T\times d}$ be a matrix with entries drawn independently from $\mathcal{N}(0, \sigma^2/d)$. The well-known DP-SGD algorithm (Abadi et al., 2016) adds this noise to each clipped gradient, so that

$$\mathbf{X} = \mathbf{X}_0 - \gamma \mathbf{A}(\overline{\mathbf{G}} + \mathbf{Z}). \tag{3}$$

$\mathbf{G}$ denotes the matrix whose rows are (stochastic) gradients $\mathbf{g}_t$ computed at the algorithm's iterates $\mathbf{x}_t$, and $\overline{\mathbf{G}}$ is the matrix formed by clipping the rows of $\mathbf{G}$ to an ℓ_2 threshold α. Note the iterates of (3) are not the same as the iterates of SGD. For consistency, we consider (2) to be the special case of (3) where $\mathbf{Z} = \mathbf{0}$ and $\alpha = \infty$. Abadi et al. (2016) derive formal DP guarantees for the output of (3) which depend in part on the variance σ^2 and the clipping threshold α.

In order to derive improved DP guarantees, (Denisov et al., 2022; Choquette-Choo et al., 2022) add noise $\mathbf{Z}$ to a factorized version of $\mathbf{A}$. Formally, for a factorization $\mathbf{A} = \mathbf{B}\mathbf{C}$ with $\mathbf{B}, \mathbf{C} \in \mathbb{R}^{T\times T}$, we can add noise to the iterates via:

$$\mathbf{X} = \mathbf{X}_0 - \gamma \mathbf{B}\left(\mathbf{C}\overline{\mathbf{G}} + \mathbf{Z}\right). \tag{4}$$

The factorization $\mathbf{B} = \mathbf{A}, \mathbf{C} = \mathbf{I}$ recovers DP-SGD (3), but better factorizations (in terms of privacy-utility trade-offs) may exist. The formulation of Eq. (4) transfers the linear optimization algorithm (2) into the setting of the matrix mechanism (Li et al., 2015), a well-studied family of mechanisms in differential privacy.

Denisov et al. (2022); Choquette-Choo et al. (2022) show that the mechanism in Eq. (4) provides a DP guarantee equivalent to a single application of the Gaussian mechanism, which can be computed tightly using numerical accounting techniques (Wang et al., 2019; Koskela et al., 2021). The DP guarantee depends on a single parameter, the "noise-multiplier", which gives the ratio of the noise added to the sensitivity of the mechanism, $\sigma/\alpha\,\mathrm{sens}(\mathbf{C})$. Here, $\mathrm{sens}(\mathbf{C})$ represents the sensitivity of the mapping $\overline{\mathbf{G}} \mapsto \mathbf{C}\overline{\mathbf{G}}$ to "adjacent" input changes. In single-epoch settings, two input matrices are adjacent if they differ by a single row (Denisov et al., 2022), so the sensitivity function is $\mathrm{sens}^2(\mathbf{C}) := \max_{i\in\{1,\dots,T\}} \|\mathbf{C}_{[:,i]}\|_2^2$, i.e. the maximum ℓ_2-squared column norm of $\mathbf{C}$. For details and extensions to multiple epochs, see (Choquette-Choo et al., 2022).

Finding good factorizations. Intuitively, a factorization $\mathbf{A} = \mathbf{B}\mathbf{C}$ is good if $\mathrm{sens}^2(\mathbf{C})$ is small and the added noise $\mathbf{B}\mathbf{Z}$ does not significantly degrade the convergence of (4). Denisov et al. (2022) bound the optimization impact of the noise by $\|\mathbf{B}\|_F^2$. Thus, a natural way to find $\mathbf{B}, \mathbf{C}$ is to minimize $\mathrm{sens}^2(\mathbf{C})\,\|\mathbf{B}\|_F^2$, or equivalently $\|\mathbf{B}\|_F^2$ subject to the constraint $\mathrm{sens}(\mathbf{C}) = 1$. Denisov et al. (2022); Choquette-Choo et al. (2022) optimize exactly this objective:

Problem 2.2 (Minimal-Norm Matrix Factorization). Given a lower triangular matrix $\mathbf{A} \in \mathbb{R}^{T\times T}$, define $\mathrm{OPT}_F(\mathbf{A}) = (\mathbf{B}, \mathbf{C})$, where $\mathbf{B}, \mathbf{C} \in \mathbb{R}^{T\times T}$ solve the following optimization problem.

$$\min_{\mathbf{B},\mathbf{C}} \|\mathbf{B}\|_F^2 \quad \text{such that} \quad \mathbf{B}\mathbf{C} = \mathbf{A}, \ \ \mathrm{sens}(\mathbf{C}) = 1. \tag{5}$$

Eq. (5) is well-studied in the privacy literature and can be solved with a variety of numerical optimization algorithms (Yuan et al., 2016; McKenna et al., 2021; Denisov et al., 2022; Choquette-Choo et al., 2022). We also note that Denisov et al. (2022) show that without loss of generality, we can assume $\mathbf{B}$ and $\mathbf{C}$ are lower triangular.

It is unclear whether (5) captures the essential convergence behavior of differentially private stochastic optimization. Our goal is to understand the impact of the noise injected in (4) on convergence. We provide an analysis of how this linearly correlated noise impacts gradient descent *as a function of* $\mathbf{B}$. We derive a tighter bound than that in (Denisov et al., 2022), and use the dependence of this bound on $\mathbf{B}$ to design better factorizations for differentially private optimization.

3. Problem Formulation

In order to study the effect of the noise $\mathbf{B}\mathbf{Z}$ on optimization dynamics, we analyze a slightly simplified objective that omits parts of the procedure in (4) that are not directly related to linear noise correlation. We do this as follows:

(I) We assume that each $\mathbf{g}_t$ is the true gradient at the point $\mathbf{x}_t$, i.e. $\mathbf{g}_t = \nabla f(\mathbf{x}_t)$.

(II) We omit gradient clipping from our analysis. Alternatively, we can view this as setting the clipping threshold $\alpha = \infty$ so that $\overline{\mathbf{G}} = \mathbf{G}$ in (4).

(III) We restrict the class $\mathcal{A}$ to SGD-type algorithms where $\mathbf{A} = \mathbf{S}$, as in Example 2.1.

We impose (I) for simplicity of presentation. Our results can be extended to stochastic gradients in a straightforward way. Restriction (II) is also for simplicity. First, clipping is not directly applied to the injected noise $\mathbf{BZ}$. Second, for bounded domains or Lipschitz f, our analysis still holds. Last, practical DP methods often use adaptive clipping (Thakkar et al., 2021) instead of fixed clipping. We are not aware of any convergence analysis of such a scheme. (III) helps decouple our results from the clipping strategy. We impose (III) in order to limit the class of algorithms $\mathcal{A}$ to a well-understood subclass. The convergence properties of (2) for general matrices $\mathbf{A}$ are not well-understood even when there is no noise ($\mathbf{Z} = \mathbf{0}$). As we discuss in Section 4, even with these simplifications, the effect of $\mathbf{BZ}$ is not well-understood.

Due to (III), we are interested in factorizations $\mathbf{BC}$ of the matrix $\mathbf{A} = \mathbf{S}$, as in Example 2.1. Then, (4) becomes

$$\mathbf{X} = \mathbf{X}_0 - \gamma\left(\mathbf{SG} + \mathbf{BZ}\right). \tag{6}$$

In vector notation, for $\mathbf{b}_0 = \mathbf{0}$ and $\mathbf{B} = [\mathbf{b}_1, \dots \mathbf{b}_T]^\top$,

$$\mathbf{x}_{t+1} = \mathbf{x}_t - \gamma\left[\nabla f(\mathbf{x}_t) + (\mathbf{b}_{t+1} - \mathbf{b}_t)^\top \mathbf{Z}\right]. \tag{7}$$

We now discuss several noteworthy special cases of (7).

Example 3.1 (PGD)**.** If $\mathbf{B} = \mathbf{S}$ (see Example 2.1) we recover SGD with uncorrelated additive noise, also known as *perturbed gradient descent* (PGD), where

$$\mathbf{x}_{t+1} = \mathbf{x}_t - \gamma\left[\nabla f(\mathbf{x}_t) + \mathbf{z}_{t+1}\right]. \tag{8}$$

The convergence rate of SGD (and therefore PGD) is well-understood in the optimization literature (e.g. see Bubeck (2015, Section 6)).

Example 3.2 (Anti-PGD)**.** By setting $\mathbf{B} = \mathbf{I}$, we get an algorithm that at every iteration adds an independent noise vector $\mathbf{z}_{t+1}$ and subtracts the previously added noise $\mathbf{z}_t$:

$$\mathbf{x}_{t+1} = \mathbf{x}_t - \gamma\left[\nabla f(\mathbf{x}_t) + \mathbf{z}_{t+1} - \mathbf{z}_t\right], \quad \mathbf{z}_0 = \mathbf{0} \tag{9}$$

Intuitively, this algorithm appears to help remove the effect of noise added in the prior round. This is (up to a learning rate factor) the *anticorrelated perturbed gradient descent* (Anti-PGD) method proposed by Orvieto et al. (2022a), who study its generalization properties.

This algorithm is in fact equivalent to SGD with randomized-smoothing (Duchi et al., 2012). The equivalence follows from defining $\tilde{\mathbf{x}}_t = \mathbf{x}_t + \gamma\mathbf{z}_t$ and rewriting (9) as

$$\tilde{\mathbf{x}}_{t+1} = \tilde{\mathbf{x}}_t - \gamma\nabla f(\tilde{\mathbf{x}}_t - \gamma\mathbf{z}_t).$$

While randomized smoothing algorithm is popular for non-smooth optimization, Vardhan & Stich (2022) analyze its convergence properties in the smooth non-convex setting.

Example 3.3 (Tree Aggregation DP-FTRL)**.** For $k \geq 1$ and $t = 2^{k-1}$, define $\mathbf{H}_k \in \mathbb{R}^{(2^k-1)\times t}$ recursively as follows:

$$\mathbf{H}_1 = \begin{pmatrix}1\end{pmatrix}, \; \mathbf{H}_{k+1} = \begin{pmatrix}\mathbf{H}_k & \mathbf{0} \\ \mathbf{0} & \mathbf{H}_k \\ \mathbf{1} & \mathbf{1}\end{pmatrix}$$

where $\mathbf{1}$ above represents an all-ones row of appropriate width. For $T = 2^{k-1}$, if $\mathbf{C} = \mathbf{H}_k$ and $\mathbf{B} = \mathbf{S}\mathbf{C}_k^\dagger$ where $\mathbf{C}_k^\dagger$ denotes a carefully chosen right pseudo-inverse of $\mathbf{C}$, then we recover the same noise matrix $\mathbf{B}$ as in the DP-FTRL algorithm with either the online or full Honaker estimator (depending on the choice of $\mathbf{C}^\dagger$) as in (Kairouz et al., 2021a; Denisov et al., 2022). We also note that $\mathbf{B}, \mathbf{C}$ are not square. This can be remedied by appropriately projecting onto $\mathbb{R}^T$. See Choquette-Choo et al. (2022, Appendix D.3) for details.

3.1. Prior Convergence Rates

Denisov et al. (2022) derive an online regret bound for (6) in the convex case against an adaptive adversary. Translating this via online-to-batch convergence implies that in the stochastic setting, the average error of the iterates $\frac{1}{T+1}\sum_{t=0}^{T}\mathbb{E}\left[f(\mathbf{x}_t) - f^\star\right]$ is upper bounded by

$$\mathcal{O}\left(\frac{\|\mathbf{x}_0 - \mathbf{x}^\star\|^2}{\gamma T} + \gamma\tilde{L}^2 + \gamma\sigma\tilde{L}\frac{\|\mathbf{B}\|_F}{\sqrt{T}}\right) \tag{10}$$

where $\tilde{L}$ is the Lipshitz constant of f. This bound is pessimistic in non-adversarial settings. For PGD (Example 3.1), (10) implies that the noise term in the convergence rate has the form $\mathcal{O}(\gamma\sigma\tilde{L}\sqrt{T})$, which diverges with T for a constant stepsize. However, one can show that SGD (and therefore PGD) achieves a faster rate of $\mathcal{O}(\gamma\sigma\tilde{L})$ in stochastic settings (Shalev-Shwartz et al., 2009).

4. Deriving Tighter Convergence Rates

There is a large space of possible factorizations in Eq. (6). As Examples 3.1, 3.2, and 3.3 showcase, the choice of factorization connects to a wide body of work on DP and optimization. It remains unclear how to select a factorization, especially since prior convergence rates are loose in stochastic settings. Thus, the minimal-norm objective in Problem 2.2 may not lead to useful factorizations for stochastic optimization. As we show in Appendix A, there are matrices $\mathbf{B}_1, \mathbf{B}_2$ such that $\|\mathbf{B}_1\|_F < \|\mathbf{B}_2\|_F$, but Eq. (6) diverges with $\mathbf{B}_1$ and converges with $\mathbf{B}_2$.

We would like convergence rates for (6) that (i) apply to any factorization and (ii) yield tight convergence rates for notable special cases. We pay special attention to PGD (Example 3.1) and Anti-PGD (Example 3.2), as they represent extremes in the space of factorizations ($\mathbf{S} = \mathbf{SI}$ and $\mathbf{S} = \mathbf{IS}$, respectively). As we will show, it is possible to use existing

theoretical tools to derive tight convergence rates for both, *but not simultaneously*. To the best of our knowledge there is no existing framework that yields tight rates for both.

Below, we discuss how to derive tight rates for PGD and Anti-PGD, and how these rates use incompatible analyses. We then develop a novel analytic framework involving *restart iterates* that allows us to not just analyze these two methods, but (6) for general factorizations. We start by formally stating our assumptions.

Assumption 4.1 (Noise)**.** The rows of the noise matrix $\mathbf{Z}$, $\mathbf{z}_1, \dots, \mathbf{z}_T$, are independent random vectors such that $\forall t$, $\mathbb{E}[\mathbf{z}_t] = \mathbf{0}$ and $\mathbb{E}\left\|\mathbf{z}_t\right\|^2 \leq \sigma^2$.

We do not assume $\tilde{L}$-Lipshitzness in our results, but we do assume L-smoothness. This is a relatively standard assumption in optimization literature (Bubeck, 2015).

Assumption 4.2 (L-smoothness)**.** The function $f : \mathbb{R}^d \to \mathbb{R}$ is differentiable, and there exists $L > 0$ such that

$$\left\|\nabla f(\mathbf{x}) - \nabla f(\mathbf{y})\right\| \leq L \left\|\mathbf{x} - \mathbf{y}\right\| \quad \forall \mathbf{x}, \mathbf{y} \in \mathbb{R}^d. \tag{11}$$

For *some* of the results we will assume convexity:

Assumption 4.3 (Convexity)**.** The function $f : \mathbb{R}^d \to \mathbb{R}$ is convex, i.e. $\forall \mathbf{x}, \mathbf{y} \in \mathbb{R}^d$,

$$f(\mathbf{x}) - f(\mathbf{y}) \leq \langle \nabla f(\mathbf{x}), \mathbf{x} - \mathbf{y} \rangle. \tag{12}$$

When assuming convexity, we also assume that the infimum of f is achieved in $\mathbb{R}^d$.

4.1. Convergence Rates for PGD and Anti-PGD

In this section we discuss the (distinct) convergence analyses of PGD and Anti-PGD, and the suboptimal results derived by trying to apply the proof technique for one to the other. We focus on the convex setting for brevity, though these analyses can be directly extended to the non-convex setting.

PGD. The convergence of PGD (Example 3.1) is well-understood since it is a special case of SGD. One can show the following.

Proposition 4.4 (Adapted from Dekel et al. (2012, Theorem 1))**.** *Under Assumptions 4.1, 4.2 and 4.3, if* $\mathbf{B} = \mathbf{S}$ *and* $\gamma < 1/2L$*, then the output of* (6) *satisfies*

$$\sum_{t=0}^{T} \frac{\mathbb{E}\left[f(\mathbf{x}_t) - f^\star\right]}{T+1} \leq \mathcal{O}\left(\frac{\left\|\mathbf{x}_0 - \mathbf{x}^\star\right\|^2}{\gamma T} + \gamma\sigma^2\right). \tag{13}$$

The proof follows from combining the update (8), standard facts about convex functions, and the fact that $\gamma < 1/2L$, to get the inequality

$$\mathbb{E}_t \left\|\mathbf{x}_{t+1} - \mathbf{x}^\star\right\|^2 \leq \left\|\mathbf{x}_t - \mathbf{x}^\star\right\|^2 - \gamma\left(f(\mathbf{x}_t) - f^\star\right) + \gamma^2\sigma^2.$$

It is left to average over iterations $0 \leq t \leq T$.

Anti-PGD. For Anti-PGD (Example 3.2), one can show the following.

Proposition 4.5. *Under Assumptions 4.1, 4.2 and 4.3, if* $\mathbf{B} = \mathbf{I}$ *and* $\gamma < 1/2L$*, then the output of* (6) *satisfies*

$$\sum_{t=0}^{T} \frac{\mathbb{E}\left[f(\mathbf{x}_t) - f^\star\right]}{T+1} \leq \mathcal{O}\left(\frac{\left\|\mathbf{x}_0 - \mathbf{x}^\star\right\|^2}{\gamma T} + L\gamma^2\sigma^2\right) \tag{14}$$

By assumption, $L\gamma < 1/2$, so the RHS of (14) is strictly smaller than the RHS of (13). While this result may be known, we were unable to find a reference, so we provide a complete proof in Appendix D. The proof utilizes perturbed iterate analysis (Mania et al., 2017). We define a *virtual sequence* $\{\tilde{\mathbf{x}}_t\}_{t=0}^T$ as follows:

$$\tilde{\mathbf{x}}_{t+1} = \tilde{\mathbf{x}}_t - \gamma\nabla f(\mathbf{x}_t), \qquad \tilde{\mathbf{x}}_0 = \mathbf{x}_0 \tag{15}$$

In other words, the $\tilde{\mathbf{x}}_t$ are the iterates produced by (6) when $\mathbf{Z} = \mathbf{0}$. We can then prove the following descent inequality:

$$\left\|\tilde{\mathbf{x}}_{t+1} - \mathbf{x}^\star\right\|^2 \leq \left\|\tilde{\mathbf{x}}_t - \mathbf{x}^\star\right\|^2 - \frac{\gamma}{2}\left(f(\mathbf{x}_t) - f^\star\right) + 2L\gamma\left\|\tilde{\mathbf{x}}_t - \mathbf{x}_t\right\|^2.$$

Because of the anti-correlation in (9), the virtual iterates $\tilde{\mathbf{x}}_t$ are close to the real iterates $\mathbf{x}_t$, as $\mathbf{x}_t - \tilde{\mathbf{x}}_t = \gamma\mathbf{z}_t$. Putting this together and averaging over t, we recover (14). See Appendix D for details.

Tightness. The noise terms (those terms involving σ^2) in (13), (14) are both tight. We show this in Appendix E on the objective $f(\mathbf{x}) = (L/2)\left\|\mathbf{x}\right\|^2$.

Difficulties in a unified analysis. The proof techniques for PGD and Anti-PGD above are notably different, and do not lead to favorable results when trying to use one of the two strategies to analyze both. For example, directly analyzing Anti-PGD using the actual iterates $\mathbf{x}_t$ of (6), we only get a convergence rate of

$$\sum_{t=0}^{T} \frac{\mathbb{E}\left[f(\mathbf{x}_t) - f^\star\right]}{T+1} \leq \mathcal{O}\left(\frac{\left\|\mathbf{x}_0 - \mathbf{x}^\star\right\|^2}{\gamma T} + \gamma\sigma^2\right).$$

Note that this is strictly worse than the Anti-PGD rate in (14). While we do not see any fundamental limit to analysing Anti-PGD directly through its iterates $\mathbf{x}_t$, we do not know of how to do so in a way that recovers the rate in (14).

On the other hand, applying the perturbed iterate analysis (via the virtual sequence $\tilde{\mathbf{x}}_t$ produced by (6) when $\mathbf{Z} = \mathbf{0}$) to PGD, we only get a convergence rate of

$$\sum_{t=0}^{T} \frac{\mathbb{E}\left[f(\mathbf{x}_t) - f^\star\right]}{T+1} \leq \mathcal{O}\left(\frac{\left\|\mathbf{x}_0 - \mathbf{x}^\star\right\|^2}{\gamma T} + LT\gamma^2\sigma^2\right).$$

This rate is strictly worse than the rate derived through a virtual sequence in (13) when $\gamma > 1/LT$. As we detail in Appendix E, this bound is actually a tight upper bound for the convergence of the virtual sequence $f(\tilde{\mathbf{x}}_t)$. However, the real sequence $\mathbf{x}_t$ converges faster than this according to (13). In short, while one can use the virtual sequence $\tilde{\mathbf{x}}_t$ to effectively analyze anti-correlated noise, such techniques do not directly yield a tight analysis of PGD.

4.2. Main Results and Analytic Techniques

In order to unify the above two proof techniques we use a modified virtual sequence with *restart iterations*. For a parameter $\tau = \tilde{\Theta}(1/L\gamma)$ (throughout, $\tilde{\mathcal{O}}$ and $\tilde{\Theta}$ hide constants and poly-logarithmic factors), we define

$$\begin{aligned} \tilde{\mathbf{x}}_{t+1} &= \tilde{\mathbf{x}}_t - \gamma \nabla f(\mathbf{x}_t) \quad \text{if } t+1 \neq 0 \bmod \tau \\ \tilde{\mathbf{x}}_{t+1} &= \mathbf{x}_{t+1} \quad \text{if } t+1 = 0 \bmod \tau. \end{aligned} \tag{16}$$

Similar to the virtual sequence in (15), $\tilde{\mathbf{x}}_t$ incorporates only unnoised gradients $\nabla f(\mathbf{x}_t)$. However, every τ iterations we reset $\tilde{\mathbf{x}}_t$ to the real iterate $\mathbf{x}_t$. This allows us to control the divergence between the virtual sequence and the real sequence (enabling a tight analysis of PGD), while still capturing the convergence benefits of anti-correlated noise (enabling a tight analysis of Anti-PGD).

The parameter τ is independent of $\mathbf{B}$, and depends only on the geometry of f and the stepsize γ. Using this machinery, we can prove convergence rates of (6) for *any* factorization $\mathbf{S} = \mathbf{BC}$. These rates involve ℓ_2 distances between the rows $\mathbf{b}_t$ of the matrix $\mathbf{B}$ (where $\mathbf{b}_0 = \mathbf{0}$ for convenience).

Theorem 4.6 (non-convex)**.** *Suppose Assumptions 4.1 and 4.2 hold, $\gamma \leq 1/4L$, and $\tau = 1/\gamma L$. Then (6) produces iterates whose average error $(T+1)^{-1}\sum_{t=0}^{T}\mathbb{E}\left\|\nabla f(\mathbf{x}_t)\right\|^2$ is upper bounded by*

$$\mathcal{O}\left(\frac{(f(\mathbf{x}_0)-f^\star)}{\gamma T} + \frac{\sigma^2}{T\tau}\times\left[\frac{1}{\tau}\sum_{t=1}^{T}\left\|\mathbf{b}_t - \mathbf{b}_{\lfloor \frac{t}{\tau}\rfloor \tau}\right\|^2 + \sum_{\substack{1\leq t\leq T\\ t=0 \bmod \tau}}\left\|\mathbf{b}_t - \mathbf{b}_{t-\tau}\right\|^2\right]\right).$$

Theorem 4.7 (convex)**.** *Under Assumptions 4.1, 4.2, and 4.3, if $\gamma \leq 1/4L$ and $\tau = \tilde{\Theta}(1/\gamma L)$, then (6) produces iterates with average error $(T+1)^{-1}\sum_{t=0}^{T}\mathbb{E}\left[f(\mathbf{x}_t) - f^\star\right]$ upper bounded by*

$$\tilde{\mathcal{O}}\left(\frac{\left\|\mathbf{x}_0 - \mathbf{x}^\star\right\|^2}{\gamma T} + \frac{\sigma^2}{TL\tau}\times\left[\frac{1}{\tau}\sum_{t=1}^{T}\left\|\mathbf{b}_t - \mathbf{b}_{\lfloor \frac{t}{\tau}\rfloor \tau}\right\|^2 + \sum_{\substack{1\leq t\leq T\\ t=0 \bmod \tau}}\left\|\mathbf{b}_t - \mathbf{b}_{t-\tau}\right\|^2 + \left\|\mathbf{b}_{\lfloor \frac{T}{\tau}\rfloor \tau}\right\|^2\right]\right).$$

We give complete proofs in Appendix C. These convergence rates consist of two terms: The first term states how fast the function would converge in the absence of the noise. The second term, the *noise term*, is the focus of our paper, as it shows how the correlated noise $\mathbf{BZ}$ affects convergence.

These rates involve only differences of rows of $\mathbf{B}$ that are at most τ iterations apart. Intuitively, we can view τ as a coarse indicator of whether an iterate $\mathbf{x}_t$ is still sensitive to the noise injected at an iteration $t' < t$. If $t > t' + \tau$, then changes in the noise added at step t are effectively uncorrelated to iteration t'.

We now consider the implications of Theorem 4.7 on the special cases in Examples 3.1, 3.2.

PGD. In this case, $\mathbf{B} = \mathbf{S}$ (Example 2.1), so if $i - j \leq \tau$ then $\left\|\mathbf{b}_i - \mathbf{b}_j\right\|^2 \leq \tau$. The noise term in the convergence rate of Theorem 4.7 is therefore upper bounded by

$$\frac{\sigma^2}{TL\tau}\left[\frac{1}{\tau}\sum_{t=1}^{T}\tau + \sum_{\substack{1\leq t\leq T\\ t=0 \bmod \tau}}\tau + T\right] = \tilde{\mathcal{O}}\left(\frac{\sigma^2}{L\tau}\right) = \tilde{\mathcal{O}}\left(\gamma\sigma^2\right)$$

This matches the tight convergence rate in Proposition 4.4.

Anti-PGD. Since $\mathbf{B} = \mathbf{I}$, for any rows $\mathbf{b}_i$, $\mathbf{b}_j$, $\left\|\mathbf{b}_i - \mathbf{b}_j\right\|^2 \leq 2$. Thus, the noise term in the convergence rate of Theorem 4.7 is upper bounded by

$$\frac{\sigma^2}{TL\tau}\left[\frac{1}{\tau}\sum_{t=1}^{T}2 + \sum_{\substack{1\leq t\leq T\\ t=0 \bmod \tau}}2 + 1\right] = \tilde{\mathcal{O}}\left(\frac{\sigma^2}{L\tau^2}\right) = \tilde{\mathcal{O}}\left(L\gamma^2\sigma^2\right)$$

where we used $\tau = \tilde{\mathcal{O}}(1/L\gamma)$. This recovers the tight convergence rate in Proposition 4.5.

5. Finding Better Factorizations

The noise term in Theorems 4.6 and 4.7 can be rewritten in matrix notation (up to multiplicative constants) as

$$\left\|\mathbf{\Lambda}_\tau \mathbf{B}\right\|_F^2 = \sum_{t=1}^{T}\left\|\boldsymbol{\lambda}_t^\top \mathbf{B}\right\|^2 = \sum_{\substack{1\leq t\leq T\\ t=0 \bmod \tau}}\left\|\mathbf{b}_t - \mathbf{b}_{t-\tau}\right\|^2 + \sum_{\substack{1\leq t\leq T\\ t\neq 0 \bmod \tau}}\left\|\frac{1}{\sqrt{\tau}}\left(\mathbf{b}_t - \mathbf{b}_{\lfloor \frac{t}{\tau}\rfloor \tau}\right)\right\|^2$$

where $\mathbf{\Lambda}_\tau = \left[\boldsymbol{\lambda}_1^\top, \ldots, \boldsymbol{\lambda}_T^\top\right]^\top \in \mathbb{R}^{T\times T}$, and we set the rows $\boldsymbol{\lambda}_t$ appropriately to select corresponding row differences of $\mathbf{B}$ with either coefficient 1 or $1/\sqrt{\tau}$ depending on the index t. We give a precise definition of $\mathbf{\Lambda}_\tau$ and an explicit example when $T = 12, \tau = 3$ in Appendix B.

Based on our results in Section 4, we propose a modified version of Problem 2.2, where we minimize $\left\|\mathbf{\Lambda}_\tau \mathbf{B}\right\|_F^2$ instead of $\left\|\mathbf{B}\right\|_F^2$. In fact, we can show that for $\mathbf{A} = \mathbf{S}$, we can

Dataset	MNIST	CIFAR-10	StackOverflow
Train Records	60,000	50,000	135,818,730
Test Records	10,000	10,000	16,586,035
Dimensionality	784	3,072	200,000
Classes	10	10	10,000
Model	Logistic	CNN	LSTM
Privacy Unit	Example	Example	User
Parameters	7,056	550,570	4,050,748
Learning Setting	Centralized	Centralized	Federated

Table 1. Summary of datasets and associated problems considered in this empirical evaluation.

solve this modified problem by first computing the solution $\tilde{\mathbf{B}}, \tilde{\mathbf{C}}$ to $\mathrm{OPT}_F(\mathbf{\Lambda}_\tau \mathbf{A})$. The solution to our modified objective is then $\mathbf{C} = \tilde{\mathbf{C}}$, $\mathbf{B} = \mathbf{A}\mathbf{C}^{-1}$. This implies we can use existing open-source solvers (Yuan et al., 2016; McKenna et al., 2021; Denisov et al., 2022).

6. Experiments

We now compare the prior methods of MF-DP-FTRL (Denisov et al., 2022; Choquette-Choo et al., 2022), and DP-SGD with privacy amplification (Abadi et al., 2016) to our method. For brevity, we refer to these as DP-MF, DP-SGD, and DP-MF$^+$, respectively. We omit from comparison DP-FTRL (Kairouz et al., 2021a) and DP-Fourier (Choquette-Choo et al., 2022) as these methods are strictly dominated by DP-MF. Unlike our analysis, we include clipping in order to derive formal (ε, δ) privacy guarantees. To facilitate a fair comparison, all methods are run with the same privacy guarantee.

Datasets and tasks. Table 1 summarizes the datasets and problems used in our empirical evaluation. For the MNIST dataset, light preprocessing is done so the 28×28 input images are flattened to size 784 vectors and normalized so entries lie in the range $[0, 1]$. For the CIFAR-10 and StackOverflow datasets, the experimental setup including data preprocessing follows exactly from Denisov et al. (2022) and Choquette-Choo et al. (2022).

Metrics. For each dataset, mechanism, and privacy parameter, we run the mechanism for multiple trials and report the test set accuracy of the final iterate. We compute the mean and standard error of the reported test set accuracies.

6.1. Experimental Results

MNIST Logistic Regression - Image Classification For MNIST, all mechanisms train for $T = 2048$ iterations and either 1 or 16 epochs.[1] We vary ε over $\{0.01, 0.1, \ldots, 100\}$ and fix $\delta = 10^{-6}$. We fix the clipping threshold at 1.0 and the learning rate at 0.5. We run each experiment for 5 trials, and plot the mean test set accuracy along with error bars indicating the standard error of the estimate. We treat τ in Section 5 as a hyper-parameter and consider $\tau = 2, 8, 32, 128, 512, 2048$. The results are given in Figs. 1(a) and 1(b). From these figures, we make the following observations:

- The performance of DP-MF$^+$ increases monotonically with τ, performing best when $\tau = T$. In Section 5, this corresponds to the objective $\|\mathbf{\Lambda}_T \mathbf{B}\|_F^2$ where $\lambda_{ii} = 1/\sqrt{T}$ for all $i < T$ and $\lambda_{TT} = 1$. This objective strongly penalizes errors on the final iterate, which is the model used to compute the test accuracy.
- When $\tau = 2048$, DP-MF$^+$ consistently out-performs DP-MF across all privacy levels and number of epochs.
- DP-MF$^+$ expands the number of settings in which we can beat DP-SGD. DP-MF only outperforms DP-SGD for sufficiently large ε ($\varepsilon \geq 0.31$ for 1 epoch and $\varepsilon \geq 31$ for 16 epochs). By contrast, DP-MF$^+$ outperforms DP-SGD in every setting except when $\varepsilon = 0.01$ and 1 epoch.
- None of the mechanisms reached the accuracy levels obtained by the non-private baseline, even at $\varepsilon = 100$. We suspect this is due to the fact that we are using a fixed but aggressive clipping threshold of 1.0 across all experiments, which helps in the moderate privacy regime but hurts in very low privacy regime.

We emphasize that DP-MF$^+$, while not relying on privacy amplification by sampling, outperforms DP-SGD baseline that benefits from privacy amplification by sampling. This is due to the efficient noise anti-correlations in the DP-MF$^+$ mechanism. In the setting where amplification is not possible, performance of DP-SGD would degrade even further.

CIFAR-10 CNN - Image Classification For CIFAR-10, we follow the experimental setup from (Choquette-Choo et al., 2022). Specifically, we train all mechanisms for 20 epochs and $T = 2000$ iterations, which corresponds to a batch size of 500.[2] We consider $\varepsilon = 1, 2, 4, 8, 16, 32$ and set $\delta = 10^{-6}$. We tune the learning rate non-privately for each method and ε by running a single trial with a fixed random seed and choosing the one which achieved the lowest training error. For each value of ε, we use the tuned

[1] In practice, one often trains small-scale models for many epochs, perhaps even using full-batch gradients, to improve the privacy/utility trade-off (at the cost of increased computation). We are interested in the *relative* performance for a fixed computation budget, so we train for a small number of epochs.

[2] While Choquette-Choo et al. (2022) use momentum and learning rate decay, we omit the use of such techniques as they are orthogonal to our theoretical results.

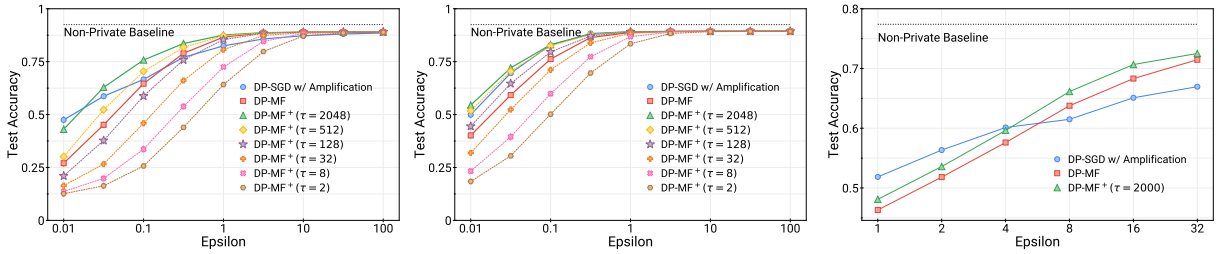

(a) MNIST, 1 epoch (b) MNIST, 16 epochs (c) CIFAR-10, 20 epochs

Figure 1. Test set accuracy of various mechanisms on the MNIST and CIFAR-10 datasets.

learning rate and run 12 new trials with different random seeds, and record the test set accuracy at the end of training. We fix $\tau = 2000$ in DP-MF$^+$ as we found that worked best in the MNIST experiments. From Fig. 1(c), we make the following observations:

- DP-MF$^+(\tau = 2000)$ offers a consistent improvement over DP-MF across all choices of ε considered.
- Both DP-MF and DP-MF$^+$ beat DP-SGD for $\varepsilon > 4$. This observation is consistent with prior work on DP-FTRL and DP-MF, where DP-SGD performs relatively better at smaller values of ε while DP-MF performs better at larger values of ε.
- Compared to the results in (Choquette-Choo et al., 2022), our test accuracies are slightly lower. This is because we train with standard SGD, while Choquette-Choo et al. (2022) use SGD with heavy-ball momentum and learning rate decay. The improvement offered by these modifications is significant. Extending our theory to such methods is a promising direction for future research.

Stackoverflow LSTM - Next Word Prediction We follow the experimental setup of Denisov et al. (2022). We train each mechanism for 1 epoch and 2048 iterations, which corresponds to about 167 clients per round, each holding an average of ≈ 400 records. We vary the hyper-parameters according to prior work and run 2 trials for each hyper-parameter setting. We report results for the best hyper-parameters setting of each mechanism. We use federated averaging instead of gradient descent. Additionally, to be consistent with the prior work and to test if our proposed factorizations are compatible with the other types of workloads, we use momentum and learning rate decay. Although the $\mathbf{C}$ matrix was optimized for the Prefix workload, $\mathbf{A} = \mathbf{S}$, it is applied to a variant $\mathbf{A} = \mathbf{S}'$ that incorporates momentum and learning rate decay by setting $\mathbf{B} = \mathbf{S}'\mathbf{C}^{-1}$. More details of how DP-MF and DP-MF$^+$ apply to this setting are available in Denisov et al. (2022).

Noise Multiplier	DP-MF	DP-MF$^+(\tau = 2048)$
0.341	24.63 ± 0.06	24.58 ± 0.12
0.682	23.76 ± 0.14	23.73 ± 0.16
1.364	22.54 ± 0.11	22.44 ± 0.08
2.728	11.51 ± 12.71	10.42 ± 13.05
5.456	0.03 ± 0.02	0.05 ± 0.06

Table 2. Comparison of test set accuracies on the Stackoverflow next word prediction task between DP-MF and DP-MF$^+$.

The results are shown in Table 2. We see no significant difference between DP-MF and DP-MF$^+$, as the small differences in performance are within the statistical bounds one would expect if they had identical means. At larger noise multipliers, both DP-MF and DP-MF$^+$ exhibit learning instabilities.

7. Conclusion and Open Questions

In this work, we developed analytic techniques to study the convergence of gradient descent under linearly correlated noise that recover tight rates for important special cases, and generally give tighter bounds than currently exist in the literature. Perhaps more importantly, our work highlights the wealth of stochastic optimization questions arising from recent advances in differentially private model training. As such, we distill and formalize various optimization problems arising from recent work on matrix mechanisms for DP.

Our work raises a host of questions and open problems, including extending our analysis to include things such as clipping, shuffling, and momentum. Another key extension is to derive last-iterate convergence rates rather than average-iterate convergence rates, as in some settings it is only the final "released" model that needs formal privacy guarantees. Given the improved generalization properties of Anti-PGD (Orvieto et al., 2022a), one could also investigate how to design more general linearly correlated noise mechanisms which improve both privacy and generalization.

References

Abadi, M., Chu, A., Goodfellow, I., McMahan, H. B., Mironov, I., Talwar, K., and Zhang, L. Deep learning with differential privacy. *Proceedings of the 2016 ACM SIGSAC Conference on Computer and Communications Security*, Oct 2016. doi: 10.1145/2976749.2978318. URL http://dx.doi.org/10.1145/2976749.2978318.

Agarwal, A. and Duchi, J. C. Distributed delayed stochastic optimization. In Shawe-Taylor, J., Zemel, R., Bartlett, P., Pereira, F., and Weinberger, K. (eds.), *Advances in Neural Information Processing Systems*, volume 24. Curran Associates, Inc., 2011. URL https://proceedings.neurips.cc/paper/2011/file/f0e52b27a7a5d6a1a87373dffa53dbe5-Paper.pdf.

Bassily, R., Smith, A., and Thakurta, A. Private empirical risk minimization: Efficient algorithms and tight error bounds. In *2014 IEEE 55th annual symposium on foundations of computer science*, pp. 464–473. IEEE, 2014.

Bassily, R., Feldman, V., Talwar, K., and Guha Thakurta, A. Private stochastic convex optimization with optimal rates. *Advances in neural information processing systems*, 32, 2019.

Bubeck, S. Convex optimization: Algorithms and complexity. *Found. Trends Mach. Learn.*, 8(3–4):231–357, nov 2015. ISSN 1935-8237. doi: 10.1561/2200000050. URL https://doi.org/10.1561/2200000050.

Chen, H., Zheng, L., Al Kontar, R., and Raskutti, G. Stochastic gradient descent in correlated settings: A study on gaussian processes. *Advances in neural information processing systems*, 33:2722–2733, 2020.

Choquette-Choo, C. A., McMahan, H. B., Rush, K., and Thakurta, A. Multi-epoch matrix factorization mechanisms for private machine learning, 2022. URL https://arxiv.org/abs/2211.06530.

Das, R., Kale, S., Xu, Z., Zhang, T., and Sanghavi, S. Beyond uniform Lipschitz condition in differentially private optimization. *arXiv preprint arXiv:2206.10713*, 2022.

Dekel, O., Gilad-Bachrach, R., Shamir, O., and Xiao, L. Optimal distributed online prediction using mini-batches. *J. Mach. Learn. Res.*, 13(null):165–202, jan 2012. ISSN 1532-4435.

Denisov, S., McMahan, B., Rush, K., Smith, A., and Thakurta, A. G. Improved differential privacy for SGD via optimal private linear operators on adaptive streams. In *Neural Information Processing Systems*, 2022.

Duchi, J. C., Bartlett, P. L., and Wainwright, M. J. Randomized smoothing for stochastic optimization. *SIAM Journal on Optimization*, 22(2):674–701, 2012.

Dutta, S., Joshi, G., Ghosh, S., Dube, P., and Nagpurkar, P. Slow and stale gradients can win the race: Error-runtime trade-offs in distributed sgd. In *International conference on artificial intelligence and statistics*, pp. 803–812. PMLR, 2018.

Dwork, C., McSherry, F., Nissim, K., and Smith, A. Calibrating noise to sensitivity in private data analysis. In Halevi, S. and Rabin, T. (eds.), *Theory of Cryptography*, pp. 265–284, Berlin, Heidelberg, 2006. Springer Berlin Heidelberg. ISBN 978-3-540-32732-5.

Edmonds, A., Nikolov, A., and Ullman, J. The power of factorization mechanisms in local and central differential privacy. In *Proceedings of the 52nd Annual ACM SIGACT Symposium on Theory of Computing*, pp. 425–438, 2020.

Erlingsson, Ú., Feldman, V., Mironov, I., Raghunathan, A., Talwar, K., and Thakurta, A. Amplification by shuffling: From local to central differential privacy via anonymity. In *Proceedings of the Thirtieth Annual ACM-SIAM Symposium on Discrete Algorithms*, pp. 2468–2479. SIAM, 2019.

Feldman, V., McMillan, A., and Talwar, K. Hiding among the clones: A simple and nearly optimal analysis of privacy amplification by shuffling. In *2021 IEEE 62nd Annual Symposium on Foundations of Computer Science (FOCS)*, pp. 954–964. IEEE, 2022.

Gorbunov, E., Kovalev, D., Makarenko, D., and Richtárik, P. Linearly converging error compensated sgd. *Advances in Neural Information Processing Systems*, 33:20889–20900, 2020.

Henzinger, M. and Upadhyay, J. Constant matters: Fine-grained complexity of differentially private continual observation using completely bounded norms. Cryptology ePrint Archive, Paper 2022/225, 2022. URL https://eprint.iacr.org/2022/225. https://eprint.iacr.org/2022/225.

Jin, C., Netrapalli, P., Ge, R., Kakade, S. M., and Jordan, M. I. On nonconvex optimization for machine learning: Gradients, stochasticity, and saddle points. *Journal of the ACM (JACM)*, 68(2):1–29, 2021.

Kairouz, P., Mcmahan, B., Song, S., Thakkar, O., Thakurta, A., and Xu, Z. Practical and private (deep) learning without sampling or shuffling. In Meila, M. and Zhang, T. (eds.), *Proceedings of the 38th International Conference on Machine Learning*, volume 139 of *Proceedings of Machine Learning Research*, pp. 5213–5225. PMLR, 18–24 Jul 2021a.

URL https://proceedings.mlr.press/v139/kairouz21b.html.

Kairouz, P., McMahan, H. B., Avent, B., Bellet, A., Bennis, M., Bhagoji, A. N., Bonawitz, K., Charles, Z., Cormode, G., Cummings, R., et al. Advances and open problems in federated learning. *Foundations and Trends® in Machine Learning*, 14(1–2):1–210, 2021b.

Karimireddy, S. P., Kale, S., Mohri, M., Reddi, S., Stich, S., and Suresh, A. T. Scaffold: Stochastic controlled averaging for federated learning. In *International Conference on Machine Learning*, pp. 5132–5143. PMLR, 2020.

Koloskova, A., Loizou, N., Boreiri, S., Jaggi, M., and Stich, S. U. A unified theory of decentralized SGD with changing topology and local updates. In *Proceedings of the 37th International Conference on Machine Learning*, ICML'20. JMLR.org, 2020.

Koskela, A., Jälkö, J., Prediger, L., and Honkela, A. Tight differential privacy for discrete-valued mechanisms and for the subsampled gaussian mechanism using FFT. In *International Conference on Artificial Intelligence and Statistics*, pp. 3358–3366. PMLR, 2021.

Li, C., Hay, M., Rastogi, V., Miklau, G., and McGregor, A. Optimizing linear counting queries under differential privacy. In *Proceedings of the twenty-ninth ACM SIGMOD-SIGACT-SIGART symposium on Principles of database systems*, pp. 123–134, 2010.

Li, C., Miklau, G., Hay, M., Mcgregor, A., and Rastogi, V. The matrix mechanism: optimizing linear counting queries under differential privacy. *The VLDB Journal*, 24: 757–781, 2015.

Lucchi, A., Proske, F., Orvieto, A., Bach, F., and Kersting, H. On the theoretical properties of noise correlation in stochastic optimization. *Neural Information Processing Systems*, 2022.

Mania, H., Pan, X., Papailiopoulos, D., Recht, B., Ramchandran, K., and Jordan, M. I. Perturbed iterate analysis for asynchronous stochastic optimization. *SIAM Journal on Optimization*, 27(4):2202–2229, 2017. doi: 10.1137/16M1057000. URL https://doi.org/10.1137/16M1057000.

McKenna, R., Miklau, G., Hay, M., and Machanavajjhala, A. Optimizing error of high-dimensional statistical queries under differential privacy. *arXiv preprint arXiv:1808.03537*, 2018.

McKenna, R., Miklau, G., Hay, M., and Machanavajjhala, A. Hdmm: Optimizing error of high-dimensional statistical queries under differential privacy. *arXiv preprint arXiv:2106.12118*, 2021.

Mishchenko, K., Khaled, A., and Richtárik, P. Random reshuffling: Simple analysis with vast improvements. *Advances in Neural Information Processing Systems*, 33: 17309–17320, 2020.

Mitra, A., Jaafar, R., Pappas, G. J., and Hassani, H. Linear convergence in federated learning: Tackling client heterogeneity and sparse gradients. *Advances in Neural Information Processing Systems*, 34:14606–14619, 2021.

Nesterov, Y. A method for solving the convex programming problem with convergence rate $o(1/k^2)$. *Proceedings of the USSR Academy of Sciences*, 269:543–547, 1983.

Nguyen, J., Malik, K., Zhan, H., Yousefpour, A., Rabbat, M., Malek, M., and Huba, D. Federated learning with buffered asynchronous aggregation. In *International Conference on Artificial Intelligence and Statistics*, pp. 3581–3607. PMLR, 2022.

Orvieto, A., Kersting, H., Proske, F., Bach, F., and Lucchi, A. Anticorrelated noise injection for improved generalization. *arXiv preprint arXiv:2202.02831*, 2022a.

Orvieto, A., Raj, A., Kersting, H., and Bach, F. Explicit regularization in overparametrized models via noise injection. *arXiv preprint arXiv:2206.04613*, 2022b.

Polyak, B. Some methods of speeding up the convergence of iteration methods. *USSR Computational Mathematics and Mathematical Physics*, 4(5):1–17, 1964. ISSN 0041-5553. doi: https://doi.org/10.1016/0041-5553(64)90137-5. URL https://www.sciencedirect.com/science/article/pii/0041555364901375.

Robbins, H. and Monro, S. A stochastic approximation method. *The Annals of Mathematical Statistics*, 22(3):400 – 407, 1951. doi: 10.1214/aoms/1177729586. URL https://doi.org/10.1214/aoms/1177729586.

Shalev-Shwartz, S., Shamir, O., Srebro, N., and Sridharan, K. Stochastic convex optimization. In *Annual Conference Computational Learning Theory*, 2009.

Stich, S. U. Local SGD converges fast and communicates little. In *International Conference on Learning Representations*, 2019. URL https://openreview.net/forum?id=S1g2JnRcFX.

Stich, S. U. and Karimireddy, S. P. The error-feedback framework: Better rates for SGD with delayed gradients and compressed updates. *J. Mach. Learn. Res.*, 21(1), jun 2022. ISSN 1532-4435.

Stich, S. U., Cordonnier, J.-B., and Jaggi, M. Sparsified SGD with memory. *Advances in Neural Information Processing Systems*, 31, 2018.

Thakkar, O., Andrew, G., and McMahan, H. B. Differentially private learning with adaptive clipping. In *Advances in Neural Information Processing Systems*, 2021.

Vardhan, H. and Stich, S. U. Tackling benign nonconvexity with smoothing and stochastic gradients, 2022. URL https://arxiv.org/abs/2202.09052.

Wang, D., Ye, M., and Xu, J. Differentially private empirical risk minimization revisited: Faster and more general. *Advances in Neural Information Processing Systems*, 30, 2017.

Wang, Y.-X., Balle, B., and Kasiviswanathan, S. P. Subsampled Rényi differential privacy and analytical moments accountant. In *The 22nd International Conference on Artificial Intelligence and Statistics*, pp. 1226–1235. PMLR, 2019.

Yu, H., Jin, R., and Yang, S. On the linear speedup analysis of communication efficient momentum sgd for distributed non-convex optimization. In *International Conference on Machine Learning*, pp. 7184–7193. PMLR, 2019.

Yuan, G., Yang, Y., Zhang, Z., and Hao, Z. Convex optimization for linear query processing under approximate differential privacy, 2016. URL https://arxiv.org/abs/1602.04302.

Yuan, H. and Ma, T. Federated accelerated stochastic gradient descent. *Advances in Neural Information Processing Systems*, 33:5332–5344, 2020.

Yun, C., Rajput, S., and Sra, S. Minibatch vs local SGD with shuffling: Tight convergence bounds and beyond. In *International Conference on Learning Representations*, 2022. URL https://openreview.net/forum?id=LdlwbBP2mlq.

Zhou, M., Liu, T., Li, Y., Lin, D., Zhou, E., and Zhao, T. Toward understanding the importance of noise in training neural networks. In *International Conference on Machine Learning*, pp. 7594–7602. PMLR, 2019.

Zhu, Y. and Wang, Y.-X. Poission subsampled Rényi differential privacy. In *International Conference on Machine Learning*, pp. 7634–7642. PMLR, 2019.

A. Additional Examples

A.1. Why the Frobenius norm is not predictive

In this section we give an explicit example of a matrix $\mathbf{B}$ for which the Frobenius norm $\|\mathbf{B}\|_F$ does not give a good estimation of the optimization behavior of (6).

Example A.1 (Chess-PGD)**.** We consider the special case of algorithm (6) whose noise correlation matrix $\mathbf{B}$ whose lower triangle has a chess board-like structure given by

$$\mathbf{B}_{\text{chess}} = \begin{pmatrix} 1 & 0 & 0 & \dots & 0 \\ 0 & 1 & 0 & \dots & 0 \\ 1 & 0 & 1 & \dots & 0 \\ \dots & & & & \\ 0 & 1 & 0 & \dots & 1 \end{pmatrix}$$

We refer to this algorithm (whose perturbed noise structure is given by $\mathbf{B}_{\text{chess}}$) as Chess-PGD. Note that $\|\mathbf{B}_{\text{chess}}\|_F < \|\mathbf{S}\|_F$. Despite this, PGD (for which $\mathbf{B} = \mathbf{S}$) converges strictly faster than Chess-PGD in Fig. 2.

By contrast, our Theorem 4.7 is better able to capture the behaviour of Chess-PGD. Suppose that $\tau \leq T/4$. Given a row $\mathbf{b}_t$ of $\mathbf{B}_{\text{chess}}$, for any $t' < t$ we have

$$\frac{t - t'}{2} \leq \|\mathbf{b}_t - \mathbf{b}_{t'}\|^2 \leq t.$$

Therefore, at least $T/4$ of the summands in the noise term of Theorem 4.7 are on the order of $\Theta(T)$. Plugging in this estimate into the convergence rate, we find that Chess-PGD produces iterates that satisfy the convergence rate

$$\frac{1}{T+1}\sum_{t=0}^{T}\mathbb{E}\left[f(\mathbf{x}_t) - f^*\right] = \tilde{\mathcal{O}}\left(\frac{\|\mathbf{x}_0 - \mathbf{x}^\star\|^2}{\gamma T} + LT\gamma^2\sigma^2\right). \tag{17}$$

Indeed, as we show below (and plot in Figure 2), Chess-PGD linearly diverges with T as predicted.

A.2. Experimental behaviour of considered examples

We implement (6) with $f(\mathbf{x}) = \frac{1}{2}\|\mathbf{Q}\mathbf{x} - \mathbf{b}\|^2$, where $\mathbf{x} \in \mathbb{R}^{100}$, $\mathbf{b} \in \mathbb{R}^{100}$ with every element $[\mathbf{b}]_i$ sampled from normal distribution $\mathcal{N}(0, 1)$, and $\mathbf{Q} \in \mathbb{R}^{100\times 100}$ is matrix with eigenvalues linearly distributed between 1 and 10. We also rotate $\mathbf{Q}$ using random unitary matrix. We set the stepsize constant, $\gamma = 0.1$.

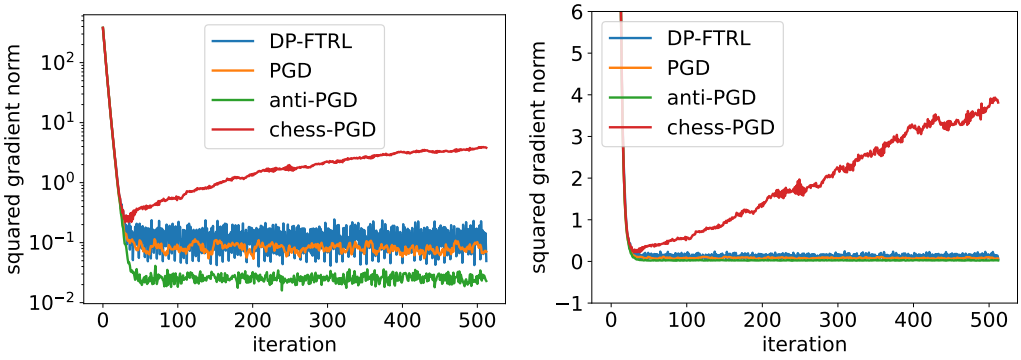

Figure 2. Behaviour of different noise patterns $\mathbf{B}$ on a quadratic function with constant stepsize, $\gamma = 0.1$. Y axis in the log scale on the left, and in the normal scale on the right.

Figure 2 compares performance of (7) with four different noise patterns $\mathbf{B}$: (i) PGD from Example 3.1, $\mathbf{B} = \mathbf{S}$ (ii) Anti-PGD from Example 3.2, $\mathbf{B} = \mathbf{I}$ (iii) DP-FTRL from Example 3.3, and (iv) Chess-PGD $\mathbf{B}_{\text{chess}}$ from Example A.1. For all methods, we plot $\|\nabla f(\mathbf{x}_t)\|^2$ at each iteration t. We see that, as predicted by (17), Chess-PGD diverges with linear rate in T, while

both PGD and Anti-PGD converge to a constant noise level. As predicted by their convergence rates, Anti-PGD has convergence with better dependence on the noise level.

We note that aim of this experiment is to illustrate theoretical bound for the simplified algorithm (7). In order to have formal privacy guarantees one should account for sensitivity of matrix $\mathbf{C}$, and clip the gradients.

B. Weight matrix

In this section we give the precise definition of the weight matrix Λ_τ (see Section 5). $\Lambda_\tau = [\lambda_{tj}]_{t,j=1,\dots,T}$ with the element

$$\lambda_{tj} = \begin{cases} \frac{1}{\sqrt{\tau}} & j = t, \quad t \neq 0 \bmod \tau \\ -\frac{1}{\sqrt{\tau}} & j = \lfloor \frac{t}{\tau} \rfloor \tau, \quad t \neq 0 \bmod \tau, t > \tau \\ 1 & j = t, \quad t = 0 \bmod \tau \\ -1 & j = t - \tau, \quad t = 0 \bmod \tau, t > \tau \end{cases}$$

For all the other indices, $\lambda_{tj} = 0$. In Figure 3 we give an example of such a matrix for $T = 12$ and $\tau = 3$.

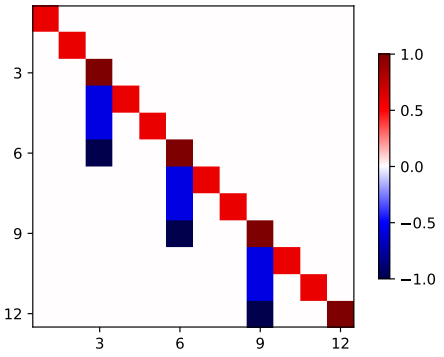

Figure 3. Elements of Λ_τ for $T = 12$, and $\tau = 3$.

C. Proofs of Main Results

We analyse the algorithm with general $\mathbf{B}$ that has the following iterates:

$$\mathbf{x}_{t+1} = \mathbf{x}_t - \eta(\nabla f(\mathbf{x}_t) + (\mathbf{b}_{t+1} - \mathbf{b}_t)^\top \mathbf{Z}) \quad t \geq 1 \tag{18}$$

where $\mathbf{b}_0 = 0$. We define $\mathbf{v}_t = (\mathbf{b}_{t+1} - \mathbf{b}_t)^\top \mathbf{Z}$ for $t \geq 0$, so that

$$\mathbf{x}_{t+1} = \mathbf{x}_t - \gamma \nabla f(\mathbf{x}_t) - \gamma \mathbf{v}_t$$

For the analysis, we define a virtual sequence with restarts (16), where we do restarts every τ iterations. Formally, we define virtual iterates $\{\tilde{\mathbf{x}}_t\}_{t=0}^T$ as follows:

$$\begin{aligned} \tilde{\mathbf{x}}_{t+1} &= \tilde{\mathbf{x}}_t - \gamma \nabla f(\mathbf{x}_t) && \text{if } t+1 \neq 0 \bmod \tau \\ \tilde{\mathbf{x}}_{t+1} &= \mathbf{x}_{t+1} && \text{if } t+1 = 0 \bmod \tau \text{ (restart iterations)} \end{aligned}$$

This means that $\tilde{\mathbf{x}}_{k\tau} = \mathbf{x}_{k\tau}$, for any nonnegative integer k.

C.1. Useful facts about this sequence.

- The closest restart iteration to t is equal to $\lfloor \frac{t}{\tau} \rfloor \tau$.
- For $t < \tau$ we have

$$\tilde{\mathbf{x}}_t - \mathbf{x}_t = \gamma \mathbf{b}_t^\top \mathbf{Z}$$

- For restart iterations $t+1=\tau$,

$$\tilde{\mathbf{x}}_{t+1}-\mathbf{x}_{t+1}=0$$

- For the next iteration just after restart $t+1=\tau+1$

$$\tilde{\mathbf{x}}_{\tau+1}-\mathbf{x}_{\tau+1}=(\tilde{\mathbf{x}}_\tau-\gamma\nabla f(\mathbf{x}_\tau))-(\mathbf{x}_\tau-\gamma\nabla f(\mathbf{x}_\tau)-\gamma\mathbf{v}_\tau)=\gamma\mathbf{v}_\tau=\gamma(\mathbf{b}_{\tau+1}-\mathbf{b}_\tau)^\top\mathbf{Z}$$

- Thus, for arbitrary t,

$$\tilde{\mathbf{x}}_t-\mathbf{x}_t=\gamma(\mathbf{b}_t-\mathbf{b}_{\lfloor\frac{t}{\tau}\rfloor\tau})^\top\mathbf{Z} \tag{19}$$

  (and if $t=0 \bmod \tau$, then the term cancels and we get $\tilde{\mathbf{x}}_t-\mathbf{x}_t=0$), we assume that $\mathbf{b}_0=\mathbf{0}$.

- We can re-write the restart iterations for $t+1=0 \bmod \tau$

$$\begin{aligned}\tilde{\mathbf{x}}_{t+1}=\mathbf{x}_{t+1}&=\mathbf{x}_t-\gamma\nabla f(\mathbf{x}_t)-\gamma(\mathbf{b}_{t+1}-\mathbf{b}_t)^\top\mathbf{Z}\\&=\tilde{\mathbf{x}}_t-\gamma\nabla f(\mathbf{x}_t)-\gamma(\mathbf{b}_t-\mathbf{b}_{\lfloor\frac{t}{\tau}\rfloor\tau})^\top\mathbf{Z}-\gamma(\mathbf{b}_{t+1}-\mathbf{b}_t)^\top\mathbf{Z}\\&=\tilde{\mathbf{x}}_t-\gamma\nabla f(\mathbf{x}_t)-\gamma(\mathbf{b}_{t+1}-\mathbf{b}_{\lfloor\frac{t}{\tau}\rfloor\tau})^\top\mathbf{Z}\end{aligned}$$

  Equivalently, for $t+1=0 \bmod \tau$,

$$\tilde{\mathbf{x}}_{t+1}=\tilde{\mathbf{x}}_t-\gamma\nabla f(\mathbf{x}_t)-\gamma(\mathbf{b}_{t+1}-\mathbf{b}_{t+1-\tau})^\top\mathbf{Z}. \tag{20}$$

C.2. Useful inequalities

Lemma C.1. *For any finite set of vectors $\{\mathbf{a}_i\}_{i=1}^n\subset\mathbb{R}^d$,*

$$\left\|\sum_{i=1}^n\mathbf{a}_i\right\|^2\le n\sum_{i=1}^n\|\mathbf{a}_i\|^2. \tag{21}$$

Lemma C.2. *For any two vectors $\mathbf{a},\mathbf{b}\in\mathbb{R}^d$ and for all $\alpha>0$,*

$$2\langle\mathbf{a},\mathbf{b}\rangle\le\alpha\|\mathbf{a}\|^2+\alpha^{-1}\|\mathbf{b}\|^2. \tag{22}$$

C.3. Proof for non-convex functions

Iterations without restarts. If t is such that $t\neq-1 \bmod \tau$, where k is some integer number, then between iteration t and $t+1$ no restart of virtual sequence happens and thus $\tilde{\mathbf{x}}_{t+1}=\tilde{\mathbf{x}}_t-\gamma\nabla f(\mathbf{x}_t)$. We follow closely standard perturbed iterate analysis (Mania et al., 2017; Stich & Karimireddy, 2022). By L-smoothness of f

$$\begin{aligned}f(\tilde{\mathbf{x}}_{t+1})&\le f(\tilde{\mathbf{x}}_t)-\gamma\langle\nabla f(\tilde{\mathbf{x}}_t),\nabla f(\mathbf{x}_t)\rangle+\frac{L\gamma^2}{2}\|\nabla f(\mathbf{x}_t)\|^2\\&\le f(\tilde{\mathbf{x}}_t)-\frac{\gamma}{2}\|\nabla f(\tilde{\mathbf{x}}_t)\|^2-\frac{\gamma}{2}\|\nabla f(\mathbf{x}_t)\|^2+\frac{\gamma L^2}{2}\|\mathbf{x}_t-\tilde{\mathbf{x}}_t\|^2\\&\overset{(19)}{\le} f(\tilde{\mathbf{x}}_t)-\frac{\gamma}{2}\|\nabla f(\tilde{\mathbf{x}}_t)\|^2-\frac{\gamma}{2}\|\nabla f(\mathbf{x}_t)\|^2+\frac{\gamma^3L^2}{2}\left\|(\mathbf{b}_t-\mathbf{b}_{\lfloor\frac{t}{\tau}\rfloor\tau})^\top\mathbf{Z}\right\|^2\end{aligned} \tag{23}$$

where on the second line we used that $-2\langle\mathbf{a},\mathbf{b}\rangle=-\|\mathbf{a}\|^2-\|\mathbf{b}\|^2+\|\mathbf{a}-\mathbf{b}\|^2$ for any $\mathbf{a},\mathbf{b}\in\mathbb{R}^d$.

Iterations with restarts. Restart happens between iteration t and $t+1$ if $t=-1 \bmod \tau$. In this case, the analysis is more involved. By L-smoothness and using update rule (20)

$$f(\tilde{\mathbf{x}}_{t+1})\le f(\tilde{\mathbf{x}}_t)-\gamma\langle\nabla f(\tilde{\mathbf{x}}_t),\nabla f(\mathbf{x}_t)+(\mathbf{b}_{t+1}-\mathbf{b}_{t+1-\tau})^\top\mathbf{Z}\rangle+\frac{L}{2}\gamma^2\left\|\nabla f(\mathbf{x}_t)+(\mathbf{b}_{t+1}-\mathbf{b}_{t+1-\tau})^\top\mathbf{Z}\right\|^2 \tag{24}$$

$$\overset{(21)}{\le} f(\tilde{\mathbf{x}}_t)-\underbrace{\gamma\langle\nabla f(\tilde{\mathbf{x}}_t),\nabla f(\mathbf{x}_t)\rangle}_{:=T_1}-\underbrace{\gamma\langle\nabla f(\tilde{\mathbf{x}}_t),(\mathbf{b}_{t+1}-\mathbf{b}_{t+1-\tau})^\top\mathbf{Z}\rangle}_{:=T_2}+L\gamma^2\|\nabla f(\mathbf{x}_t)\|^2+L\gamma^2\left\|(\mathbf{b}_{t+1}-\mathbf{b}_{t+1-\tau})^\top\mathbf{Z}\right\|^2 \tag{25}$$

We estimate separately the second and the third terms

$$\begin{aligned}T_1 &= -\frac{\gamma}{2}\left\|\nabla f(\tilde{\mathbf{x}}_t)\right\|^2 - \frac{\gamma}{2}\left\|\nabla f(\mathbf{x}_t)\right\|^2 + \frac{\gamma}{2}\left\|\nabla f(\tilde{\mathbf{x}}_t) - \nabla f(\mathbf{x}_t)\right\|^2 \\ &\overset{(11)}{\leq} -\frac{\gamma}{2}\left\|\nabla f(\tilde{\mathbf{x}}_t)\right\|^2 - \frac{\gamma}{2}\left\|\nabla f(\mathbf{x}_t)\right\|^2 + \frac{\gamma L^2}{2}\left\|\tilde{\mathbf{x}}_t - \mathbf{x}_t\right\|^2 \\ &\overset{(19)}{\leq} -\frac{\gamma}{2}\left\|\nabla f(\tilde{\mathbf{x}}_t)\right\|^2 - \frac{\gamma}{2}\left\|\nabla f(\mathbf{x}_t)\right\|^2 + \frac{\gamma^3 L^2}{2}\left\|(\mathbf{b}_t - \mathbf{b}_{\lfloor \frac{t}{\tau}\rfloor \tau})^\top \mathbf{Z}\right\|^2\end{aligned}$$

The third term,

$$T_2 = -\langle \nabla f(\tilde{\mathbf{x}}_t), \gamma(\mathbf{b}_{t+1} - \mathbf{b}_{t+1-\tau})^\top \mathbf{Z}\rangle \overset{(22),\ \alpha=\frac{1}{8L}}{\leq} \frac{1}{16L}\left\|\nabla f(\tilde{\mathbf{x}}_t)\right\|^2 + 4L\gamma^2\left\|(\mathbf{b}_{t+1} - \mathbf{b}_{t+1-\tau})^\top \mathbf{Z}\right\|^2$$

It is left to deal with the norm of the gradient $\frac{1}{16L}\left\|\nabla f(\tilde{\mathbf{x}}_t)\right\|^2$. Using that $\tau = \frac{1}{L\gamma}$, and thus $\frac{1}{16L\tau} = \frac{\gamma}{16}$ we have

$$\begin{aligned}\frac{1}{16L}\left\|\nabla f(\tilde{\mathbf{x}}_t)\right\|^2 &= \frac{\gamma}{16}\sum_{i=0}^{\tau-1}\left\|\nabla f(\tilde{\mathbf{x}}_t)\right\|^2 \\ &\overset{(21),(11)}{\leq} \frac{\gamma}{8}\sum_{i=0}^{\tau-1} L^2\left\|\tilde{\mathbf{x}}_t - \tilde{\mathbf{x}}_{t-i}\right\|^2 + \frac{\gamma}{8}\sum_{i=0}^{\tau-1}\left\|\nabla f(\tilde{\mathbf{x}}_{t-i})\right\|^2 \\ &\overset{(??)}{\leq} \frac{\gamma}{8}\sum_{i=1}^{\tau-1}\gamma^2 L^2\left\|\sum_{j=t-i}^{t-1}\nabla f(\mathbf{x}_j)\right\|^2 + \frac{\gamma}{8}\sum_{i=0}^{\tau-1}\left\|\nabla f(\tilde{\mathbf{x}}_{t-i})\right\|^2 \\ &\overset{(21)}{\leq} \frac{\gamma^3 L^2}{8}\sum_{i=1}^{\tau-1}\tau\sum_{j=t-i}^{t-1}\left\|\nabla f(\mathbf{x}_j)\right\|^2 + \frac{\gamma}{8}\sum_{i=0}^{\tau-1}\left\|\nabla f(\tilde{\mathbf{x}}_{t-i})\right\|^2 \\ &\leq \frac{\gamma^3 L^2\tau^2}{8}\sum_{i=1}^{\tau-1}\left\|\nabla f(\mathbf{x}_{t-i})\right\|^2 + \frac{\gamma}{8}\sum_{i=0}^{\tau-1}\left\|\nabla f(\tilde{\mathbf{x}}_{t-i})\right\|^2 \\ &\overset{\tau=\frac{1}{\gamma L}}{\leq} \frac{\gamma}{8}\sum_{i=1}^{\tau-1}\left\|\nabla f(\mathbf{x}_{t-i})\right\|^2 + \frac{\gamma}{8}\sum_{i=0}^{\tau-1}\left\|\nabla f(\tilde{\mathbf{x}}_{t-i})\right\|^2\end{aligned}$$

Putting back our calculations of T_1 and T_2 into (25), and setting $\gamma \leq \frac{1}{4L}$ in order to estimate that $L\gamma^2\left\|\nabla f(\mathbf{x}_t)\right\|^2 \leq \frac{\gamma}{4}\left\|\nabla f(\mathbf{x}_t)\right\|^2$

$$\begin{aligned}f(\tilde{\mathbf{x}}_{t+1}) \leq f(\tilde{\mathbf{x}}_t) &- \frac{\gamma}{2}\left\|\nabla f(\tilde{\mathbf{x}}_t)\right\|^2 - \frac{\gamma}{4}\left\|\nabla f(\mathbf{x}_t)\right\|^2 + \frac{\gamma^3 L^2}{2}\left\|(\mathbf{b}_t - \mathbf{b}_{\lfloor \frac{t}{\tau}\rfloor \tau})^\top \mathbf{Z}\right\|^2 \\ &+ 5L\gamma^2\left\|(\mathbf{b}_{t+1} - \mathbf{b}_{t+1-\tau})^\top \mathbf{Z}\right\|^2 + \frac{\gamma}{8}\sum_{i=1}^{\tau-1}\left\|\nabla f(\mathbf{x}_{t-i})\right\|^2 + \frac{\gamma}{8}\sum_{i=0}^{\tau-1}\left\|\nabla f(\tilde{\mathbf{x}}_{t-i})\right\|^2\end{aligned} \tag{26}$$

Combining iterations with and without restarts. It is left to average equations (23) and (26) over all iterations $0 \leq t \leq T$. We denote $\mathcal{T}_1$ is the set of indices without restarts, and $\mathcal{T}_2$ are restarts indices.

$$\begin{aligned}&\sum_{t\in\mathcal{T}_1}\frac{\gamma}{8}\left(\left\|\nabla f(\tilde{\mathbf{x}}_t)\right\|^2 + \left\|\nabla f(\mathbf{x}_t)\right\|^2\right) + \sum_{t\in\mathcal{T}_2}\frac{\gamma}{8}\left(\left\|\nabla f(\tilde{\mathbf{x}}_t)\right\|^2 + \left\|\nabla f(\mathbf{x}_t)\right\|^2\right) \\ &\qquad \leq (f(\mathbf{x}_0) - f^\star) + \frac{\gamma^3 L^2}{2}\sum_{t=1}^{T}\left\|(\mathbf{b}_t - \mathbf{b}_{\lfloor \frac{t}{\tau}\rfloor \tau})^\top \mathbf{Z}\right\|^2 + 5L\gamma^2\sum_{t\in\mathcal{T}_1}\left\|(\mathbf{b}_{t+1} - \mathbf{b}_{t+1-\tau})^\top \mathbf{Z}\right\|^2\end{aligned}$$

Dividing by $\frac{\gamma(T+1)}{8}$, we get

$$\frac{1}{T+1}\sum_{t=0}^{T}\mathbb{E}\left\|\nabla f(\mathbf{x}_t)\right\|^2 \leq \frac{8(f(\mathbf{x}_0)-f^\star)}{\gamma(T+1)} + \frac{4\gamma^2L^2}{T+1}\sum_{t=1}^{T}\mathbb{E}\left\|(\mathbf{b}_t-\mathbf{b}_{\lfloor\frac{t}{\tau}\rfloor\tau})^\top\mathbf{Z}\right\|^2 + \frac{40L\gamma}{T+1}\sum_{k=1}^{\lfloor\frac{T}{\tau}\rfloor}\mathbb{E}\left\|(\mathbf{b}_{k\tau}-\mathbf{b}_{(k-1)\tau})^\top\mathbf{Z}\right\|^2$$

which completes the proof.

C.4. Proof for convex functions

Our proof for convex functions follows the same pattern as for non-convex: we consider separately iterations with and without restarts of the virtual sequence (16). However, summing up these two cases is the most involved part of the proof in the convex case, and it is different from the non-convex case.

We will use the following fact in our proof.

Lemma C.3. *If function f is convex (12), L-smooth (11), and has a finite minimizer x^*, then*

$$\left\|\nabla f(\mathbf{x})\right\|^2 \leq 2L\left(f(\mathbf{x})-f^\star\right). \tag{27}$$

Iterations without restarts. Using (16), i.e. that $\tilde{\mathbf{x}}_{t+1}=\tilde{\mathbf{x}}_t-\gamma\nabla f(\mathbf{x}_t)$, for some point $\mathbf{x}^\star$ that satisfies $\nabla f(\mathbf{x}^\star)=0$,

$$\begin{aligned}\left\|\tilde{\mathbf{x}}_{t+1}-\mathbf{x}^\star\right\|^2 &= \left\|\tilde{\mathbf{x}}_t-\mathbf{x}^\star\right\|^2 - 2\gamma\langle\nabla f(\mathbf{x}_t),\mathbf{x}_t-\mathbf{x}^\star\rangle + \gamma^2\left\|\nabla f(\mathbf{x}_t)\right\|^2 + 2\gamma\langle\nabla f(\mathbf{x}_t),\mathbf{x}_t-\tilde{\mathbf{x}}_t\rangle\\ &\overset{(27),(12)}{\leq} \left\|\tilde{\mathbf{x}}_t-\mathbf{x}^\star\right\|^2 - 2\gamma(1-L\gamma)\left(f(\mathbf{x}_t)-f^\star\right) + 2\gamma\langle\nabla f(\mathbf{x}_t),\mathbf{x}_t-\tilde{\mathbf{x}}_t\rangle\end{aligned}$$

We estimate the last term separately

$$2\langle\nabla f(\mathbf{x}_t),\mathbf{x}_t-\tilde{\mathbf{x}}_t\rangle \overset{(22),\alpha=2L}{\leq} \frac{1}{2L}\left\|\nabla f(\mathbf{x}_t)\right\|^2 + 2L\left\|\mathbf{x}_t-\tilde{\mathbf{x}}_t\right\|^2 \overset{(27)}{\leq} \left(f(\mathbf{x}_t)-f^\star\right) + 2L\left\|\mathbf{x}_t-\tilde{\mathbf{x}}_t\right\|^2$$

Thus,

$$\begin{aligned}\left\|\tilde{\mathbf{x}}_{t+1}-\mathbf{x}^\star\right\|^2 &\leq \left\|\tilde{\mathbf{x}}_t-\mathbf{x}^\star\right\|^2 - \gamma(1-2L\gamma)(f(\mathbf{x}_t)-f^\star) + 2L\gamma\left\|\mathbf{x}_t-\tilde{\mathbf{x}}_t\right\|^2\\ &\overset{\gamma<\frac{1}{4L},(19)}{\leq} \left\|\tilde{\mathbf{x}}_t-\mathbf{x}^\star\right\|^2 - \frac{\gamma}{2}(f(\mathbf{x}_t)-f^\star) + 2L\gamma^3\left\|(\mathbf{b}_t-\mathbf{b}_{\lfloor\frac{t}{\tau}\rfloor\tau})^\top\mathbf{Z}\right\|^2\end{aligned} \tag{28}$$

For the iterations with restarts. This means that $t+1=k\tau$. Using (20),

$$\begin{aligned}\left\|\tilde{\mathbf{x}}_{t+1}-\mathbf{x}^\star\right\|^2 &= \left\|\tilde{\mathbf{x}}_t-\mathbf{x}^\star-\gamma\nabla f(\mathbf{x}_t)-\gamma(\mathbf{b}_{t+1}-\mathbf{b}_{t+1-\tau})^\top\mathbf{Z}\right\|^2\\ &= \left\|\tilde{\mathbf{x}}_t-\mathbf{x}^\star\right\|^2 - 2\gamma\langle\nabla f(\mathbf{x}_t),\tilde{\mathbf{x}}_t-\mathbf{x}^\star\rangle - 2\gamma\langle(\mathbf{b}_{t+1}-\mathbf{b}_{t+1-\tau})^\top\mathbf{Z},\tilde{\mathbf{x}}_t-\mathbf{x}^\star\rangle + \gamma^2\left\|\nabla f(\mathbf{x}_t)+(\mathbf{b}_{t+1}-\mathbf{b}_{t+1-\tau})^\top\mathbf{Z}\right\|^2\end{aligned}$$

We estimate the second term same as in the case without restarts:

$$\begin{aligned}-2\gamma\langle\nabla f(\mathbf{x}_t),\tilde{\mathbf{x}}_t-\mathbf{x}^\star\rangle &= -2\gamma\langle\nabla f(\mathbf{x}_t),\mathbf{x}_t-\mathbf{x}^\star\rangle - 2\gamma\langle\nabla f(\mathbf{x}_t),\tilde{\mathbf{x}}_t-\mathbf{x}_t\rangle\\ &\leq -\gamma(f(\mathbf{x}_t)-f^\star) + 2L\gamma\left\|\mathbf{x}_t-\tilde{\mathbf{x}}_t\right\|^2\end{aligned}$$

For the last term,

$$\begin{aligned}\gamma^2\left\|\nabla f(\mathbf{x}_t)+(\mathbf{b}_{t+1}-\mathbf{b}_{t+1-\tau})^\top\mathbf{Z}\right\|^2 &\overset{(21)}{\leq} 2\gamma^2\left\|\nabla f(\mathbf{x}_t)\right\|^2 + 2\gamma^2\left\|(\mathbf{b}_{t+1}-\mathbf{b}_{t+1-\tau})^\top\mathbf{Z}\right\|^2\\ &\overset{(27)}{\leq} 4L\gamma^2(f(\mathbf{x}_t)-f^\star) + 2\gamma^2\left\|(\mathbf{b}_{t+1}-\mathbf{b}_{t+1-\tau})^\top\mathbf{Z}\right\|^2\end{aligned}$$

Thus with $\gamma\leq\frac{1}{8L}$,

$$\begin{aligned}\frac{\gamma}{2}(f(\mathbf{x}_t)-f^\star) \leq \left\|\tilde{\mathbf{x}}_t-\mathbf{x}^\star\right\|^2 - \left\|\tilde{\mathbf{x}}_{t+1}-\mathbf{x}^\star\right\|^2 + 2L\gamma^3\left\|(\mathbf{b}_t-\mathbf{b}_{\lfloor\frac{t}{\tau}\rfloor\tau})^\top\mathbf{Z}\right\|^2 + 2\gamma^2\left\|(\mathbf{b}_{t+1}-\mathbf{b}_{t+1-\tau})^\top\mathbf{Z}\right\|^2\\ - 2\gamma\langle(\mathbf{b}_{t+1}-\mathbf{b}_{t+1-\tau})^\top\mathbf{Z},\tilde{\mathbf{x}}_t-\mathbf{x}^\star\rangle\end{aligned} \tag{29}$$

Combining iterations with and without restarts. Summing up (28) and (29) for all $0 \leq t \leq T$,

$$\frac{\gamma}{2}\sum_{t=0}^{T}(f(\mathbf{x}_t)-f^\star) \leq \|\tilde{\mathbf{x}}_0-\mathbf{x}^\star\|^2 - \|\tilde{\mathbf{x}}_{T+1}-\mathbf{x}^\star\|^2 + 2L\gamma^3\sum_{t=0}^{T}\left\|(\mathbf{b}_t-\mathbf{b}_{\lfloor\frac{t}{\tau}\rfloor\tau})^\top\mathbf{Z}\right\|^2 + 2\gamma^2\sum_{k=1}^{\lfloor\frac{T}{\tau}\rfloor}\mathbb{E}\left\|(\mathbf{b}_{k\tau}-\mathbf{b}_{(k-1)\tau})^\top\mathbf{Z}\right\|^2 \underbrace{-2\gamma\sum_{k=1}^{\lfloor\frac{T}{\tau}\rfloor}\langle(\mathbf{b}_{k\tau}-\mathbf{b}_{(k-1)\tau})^\top\mathbf{Z},\tilde{\mathbf{x}}_{k\tau-1}-\mathbf{x}^\star\rangle}_{:=S_1} \tag{30}$$

We now separately estimate the last sum S_1. We first divide it in pairs of two consecutive terms, and sum each pair separately. Lets denote $t = k\tau - 1$ for some k. Sum of two consecutive terms with indexes t and $t-\tau$ is equal to

$$\begin{aligned}
&-2\gamma\langle(\mathbf{b}_{t+1}-\mathbf{b}_{t+1-\tau})^\top\mathbf{Z},\tilde{\mathbf{x}}_t-\mathbf{x}^\star\rangle - 2\gamma\langle(\mathbf{b}_{t+1-\tau}-\mathbf{b}_{t+1-2\tau})^\top\mathbf{Z},\tilde{\mathbf{x}}_{t-\tau}-\mathbf{x}^\star\rangle\\
=&-2\gamma\langle(\mathbf{b}_{t+1}-\mathbf{b}_{t+1-\tau})^\top\mathbf{Z},\tilde{\mathbf{x}}_t-\mathbf{x}^\star\rangle - 2\gamma\langle(\mathbf{b}_{t+1-\tau}-\mathbf{b}_{t+1-2\tau})^\top\mathbf{Z},\tilde{\mathbf{x}}_t-\mathbf{x}^\star\rangle - 2\gamma\langle(\mathbf{b}_{t+1-\tau}-\mathbf{b}_{t+1-2\tau})^\top\mathbf{Z},\tilde{\mathbf{x}}_{t-\tau}-\tilde{\mathbf{x}}_t\rangle\\
=&-2\gamma\langle(\mathbf{b}_{t+1}-\mathbf{b}_{t+1-2\tau})^\top\mathbf{Z},\tilde{\mathbf{x}}_t-\mathbf{x}^\star\rangle - 2\gamma\langle(\mathbf{b}_{t+1-\tau}-\mathbf{b}_{t+1-2\tau})^\top\mathbf{Z},\tilde{\mathbf{x}}_{t-\tau}-\tilde{\mathbf{x}}_t\rangle
\end{aligned}$$

Using update rules (16), it holds that $\tilde{\mathbf{x}}_t = \tilde{\mathbf{x}}_{t-\tau} - \gamma\sum_{j=t-\tau}^{t-1}\nabla f(\mathbf{x}_j) - \gamma(\mathbf{b}_{t+1-\tau}-\mathbf{b}_{t+1-2\tau})^\top\mathbf{Z}$, and thus

$$\begin{aligned}
-2\gamma\langle(\mathbf{b}_{t+1-\tau}-\mathbf{b}_{t+1-2\tau})^\top\mathbf{Z},&\tilde{\mathbf{x}}_{t-\tau}-\tilde{\mathbf{x}}_t\rangle = -2\gamma^2\langle(\mathbf{b}_{t+1-\tau}-\mathbf{b}_{t+1-2\tau})^\top\mathbf{Z},\sum_{j=t-\tau}^{t-1}\nabla f(\mathbf{x}_j)+(\mathbf{b}_{t+1-\tau}-\mathbf{b}_{t+1-2\tau})^\top\mathbf{Z}\rangle\\
&= \sum_{j=t-\tau}^{t-1} -2\gamma^2\langle(\mathbf{b}_{t+1-\tau}-\mathbf{b}_{t+1-2\tau})^\top\mathbf{Z},\nabla f(\mathbf{x}_j)\rangle - 2\gamma^2\left\|(\mathbf{b}_{t+1-\tau}-\mathbf{b}_{t+1-2\tau})^\top\mathbf{Z}\right\|^2\\
&\overset{(22)}{\leq} \gamma^2\alpha\tau\left\|(\mathbf{b}_{t+1-\tau}-\mathbf{b}_{t+1-2\tau})^\top\mathbf{Z}\right\|^2 + \gamma^2\alpha^{-1}\sum_{j=t-\tau}^{t-1}\|\nabla f(\mathbf{x}_t)\|^2 - 2\gamma^2\left\|(\mathbf{b}_{t+1-\tau}-\mathbf{b}_{t+1-2\tau})^\top\mathbf{Z}\right\|^2\\
&\overset{\alpha=\frac{2}{\tau}}{\leq} \frac{\gamma^2\tau}{2}\sum_{j=t-\tau}^{t-1}\|\nabla f(\mathbf{x}_t)\|^2
\end{aligned}$$

Using these calculations, our original sum S_1 can be simplified as

$$S_1 \leq -2\gamma\sum_{k=1}^{\lfloor\frac{T}{2\tau}\rfloor}\langle(\mathbf{b}_{k\cdot 2\tau}-\mathbf{b}_{(k-1)2\tau})^\top\mathbf{Z},\tilde{\mathbf{x}}_{k\cdot 2\tau-1}-\mathbf{x}^\star\rangle + \frac{\gamma^2\tau}{2}\sum_{t=0}^{\lfloor\frac{T}{\tau}\rfloor\tau-2}\|\nabla f(\mathbf{x}_t)\|^2$$

We reduced the sum of $\lfloor\frac{T}{\tau}\rfloor$ elements twice to the sum of the $\lfloor\frac{T}{2\tau}\rfloor$ elements. Continuing in similar way, we will need to have $\log_2\left(\lfloor\frac{T}{\tau}\rfloor\right)$ times until we reduce the original sum to just one element. Thus,

$$\begin{aligned}
S_1 &\leq -2\gamma\langle\mathbf{b}_{\lfloor\frac{T}{\tau}\rfloor\tau}^\top\mathbf{Z},\tilde{\mathbf{x}}_{\lfloor\frac{T}{\tau}\rfloor\tau}-\mathbf{x}^\star\rangle + \frac{\gamma^2\tau}{2}\log_2\left(\left\lfloor\frac{T}{\tau}\right\rfloor\right)\sum_{t=0}^{\lfloor\frac{T}{\tau}\rfloor\tau-2}\|\nabla f(\mathbf{x}_t)\|^2\\
&\overset{(22),\alpha=2}{\leq} \frac{1}{3}\left\|\tilde{\mathbf{x}}_{\lfloor\frac{T}{\tau}\rfloor\tau}-\mathbf{x}^\star\right\|^2 + 3\gamma^2\left\|\mathbf{b}_{\lfloor\frac{T}{\tau}\rfloor\tau}^\top\mathbf{Z}\right\|^2 + \frac{\gamma^2\tau}{2}\log_2\left(\left\lfloor\frac{T}{\tau}\right\rfloor\right)\sum_{t=0}^{\lfloor\frac{T}{\tau}\rfloor\tau-2}\|\nabla f(\mathbf{x}_t)\|^2
\end{aligned}$$

We further transform the first term using the update rule (16)

$$\tilde{\mathbf{x}}_{T+1} = \tilde{\mathbf{x}}_{\lfloor\frac{T}{\tau}\rfloor\tau} - \gamma\sum_{j=\lfloor\frac{T}{\tau}\rfloor\tau}^{T}\nabla f(\mathbf{x}_j) = \tilde{\mathbf{x}}_{\lfloor\frac{T}{\tau}\rfloor\tau-1} - \gamma\sum_{j=\lfloor\frac{T}{\tau}\rfloor\tau-1}^{T}\nabla f(\mathbf{x}_j) - \gamma\left(\mathbf{b}_{\lfloor\frac{T}{\tau}\rfloor\tau}-\mathbf{b}_{(\lfloor\frac{T}{\tau}\rfloor-1)\tau}\right)^\top\mathbf{Z}$$

Thus,

$$\frac{1}{3}\left\|\tilde{\mathbf{x}}_{\lfloor\frac{T}{\tau}\rfloor\tau}-\mathbf{x}^\star\right\|^2 \leq \|\tilde{\mathbf{x}}_{T+1}-\mathbf{x}^\star\|^2 + \gamma^2\tau\sum_{j=\lfloor\frac{T}{\tau}\rfloor\tau-1}^{T}\|\nabla f(\mathbf{x}_j)\|^2 + \gamma^2\left\|\left(\mathbf{b}_{\lfloor\frac{T}{\tau}\rfloor\tau}-\mathbf{b}_{(\lfloor\frac{T}{\tau}\rfloor-1)\tau}\right)^\top\mathbf{Z}\right\|^2$$

And thus,

$$S_1 \leq \|\tilde{\mathbf{x}}_{T+1} - \mathbf{x}^\star\|^2 + 3\gamma^2 \left\|\mathbf{b}_{\lfloor \frac{T}{\tau} \rfloor \tau}^\top \mathbf{Z}\right\|^2 + \gamma^2 \tau \log_2\left(\left\lfloor \frac{T}{\tau} \right\rfloor\right) \sum_{t=0}^{T} \|\nabla f(\mathbf{x}_t)\|^2 + \gamma^2 \left\|\left(\mathbf{b}_{\lfloor \frac{T}{\tau} \rfloor \tau} - \mathbf{b}_{(\lfloor \frac{T}{\tau} \rfloor - 1)\tau}\right)^\top \mathbf{Z}\right\|^2$$

Choosing $\tau = \frac{1}{8L\gamma \log_2(T)}$ ensures that $\gamma^2 \tau \log_2\left(\lfloor \frac{T}{\tau} \rfloor\right) \leq \frac{\gamma}{8L}$. Putting these calculations back into (30), we get that

$$\frac{\gamma}{2}\sum_{t=0}^{T}(f(\mathbf{x}_t) - f^\star) \leq \|\tilde{\mathbf{x}}_0 - \mathbf{x}^\star\|^2 + 3L\gamma^3 \sum_{t=0}^{T} \left\|(\mathbf{b}_{t-1} - \mathbf{b}_{\lfloor \frac{t}{\tau} \rfloor \tau})^\top \mathbf{Z}\right\|^2 + 3\gamma^2 \sum_{k=1}^{\lfloor \frac{T}{\tau} \rfloor} \mathbb{E}\left\|(\mathbf{b}_{k\tau} - \mathbf{b}_{(k-1)\tau})^\top \mathbf{Z}\right\|^2$$
$$+ \frac{\gamma}{8L}\sum_{t=0}^{T} \|\nabla f(\mathbf{x}_t)\|^2 + 3\gamma^2 \left\|\mathbf{b}_{\lfloor \frac{T}{\tau} \rfloor \tau}^\top \mathbf{Z}\right\|^2$$

Using (27), we can further simplify

$$\frac{\gamma}{4}\sum_{t=0}^{T}(f(\mathbf{x}_t) - f^\star) \leq \|\mathbf{x}_0 - \mathbf{x}^\star\|^2 + 3\gamma^2 \left(L\gamma \sum_{t=0}^{T} \left\|(\mathbf{b}_t - \mathbf{b}_{\lfloor \frac{t}{\tau} \rfloor \tau})^\top \mathbf{Z}\right\|^2 + \sum_{k=1}^{\lfloor \frac{T}{\tau} \rfloor} \mathbb{E}\left\|(\mathbf{b}_{k\tau} - \mathbf{b}_{(k-1)\tau})^\top \mathbf{Z}\right\|^2 + \left\|\mathbf{b}_{\lfloor \frac{T}{\tau} \rfloor \tau}^\top \mathbf{Z}\right\|^2 \right)$$

D. Convergence of Anti-PGD Example 3.2

Using that $\tilde{\mathbf{x}}_{t+1} = \tilde{\mathbf{x}}_t - \gamma \nabla f(\mathbf{x}_t)$, for some point $\mathbf{x}^\star$ that satisfies $\nabla f(\mathbf{x}^\star) = 0$,

$$\begin{aligned}\|\tilde{\mathbf{x}}_{t+1} - \mathbf{x}^\star\|^2 &= \|\tilde{\mathbf{x}}_t - \mathbf{x}^\star\|^2 - 2\gamma\langle \nabla f(\mathbf{x}_t), \mathbf{x}_t - \mathbf{x}^\star\rangle + \gamma^2 \|\nabla f(\mathbf{x}_t)\|^2 + 2\gamma\langle \nabla f(\mathbf{x}_t), \mathbf{x}_t - \tilde{\mathbf{x}}_t\rangle \\ &\overset{(27),(12)}{\leq} \|\tilde{\mathbf{x}}_t - \mathbf{x}^\star\|^2 - 2\gamma(1 - L\gamma)\left(f(\mathbf{x}_t) - f^\star\right) + 2\gamma\langle \nabla f(\mathbf{x}_t), \mathbf{x}_t - \tilde{\mathbf{x}}_t\rangle\end{aligned}$$

We estimate the last term separately

$$2\langle \nabla f(\mathbf{x}_t), \mathbf{x}_t - \tilde{\mathbf{x}}_t\rangle \overset{(22),\alpha=2L}{\leq} \frac{1}{2L}\|\nabla f(\mathbf{x}_t)\|^2 + 2L\|\mathbf{x}_t - \tilde{\mathbf{x}}_t\|^2 \overset{(27)}{\leq} (f(\mathbf{x}_t) - f^\star) + 2L\|\mathbf{x}_t - \tilde{\mathbf{x}}_t\|^2$$

Thus,

$$\begin{aligned}\|\tilde{\mathbf{x}}_{t+1} - \mathbf{x}^\star\|^2 &\leq \|\tilde{\mathbf{x}}_t - \mathbf{x}^\star\|^2 - \gamma(1 - 2L\gamma)(f(\mathbf{x}_t) - f^\star) + 2L\gamma\|\mathbf{x}_t - \tilde{\mathbf{x}}_t\|^2 \\ &\overset{\gamma < \frac{1}{4L},(19)}{\leq} \|\tilde{\mathbf{x}}_t - \mathbf{x}^\star\|^2 - \frac{\gamma}{2}(f(\mathbf{x}_t) - f^\star) + 2L\gamma\|\mathbf{x}_t - \tilde{\mathbf{x}}_t\|^2\end{aligned}$$

E. Noise Lower Bound

We consider function $f(\mathbf{x}) = \frac{L}{2}\|\mathbf{x}\|^2$ that is convex and L-smooth, and we are running algorithm (7) with constant stepsize γ, and we consider the two cases of $\mathbf{B} = \mathbf{S}$ and $\mathbf{B} = \mathbf{I}$.

E.1. PGD

This corresponds to Example 3.1. We will prove the lower bound on the noise term under the condition that T is large enough, i.e. $T \geq \frac{\log 2}{\eta L}$.

Since $\nabla f(\mathbf{x}) = L\mathbf{x}$, the algorithm (7) takes a form

$$\mathbf{x}_{t+1} = (1 - \gamma L)\mathbf{x}_t - \gamma \mathbf{z}_{t+1}$$

Thus, since $\mathbf{x}^\star = 0$,

$$\mathbb{E}\|\mathbf{x}_{t+1}\|^2 = \mathbb{E}\|(1 - \gamma L)\mathbf{x}_t - \gamma \mathbf{z}_{t+1}\|^2 = (1 - \gamma L)^2\|\mathbf{x}_t\|^2 + \gamma^2\sigma^2 = (1 - \gamma L)^{2(t+1)}\|\mathbf{x}_0\|^2 + \gamma^2\sigma^2 \sum_{j=0}^{t}(1 - \gamma L)^{2j}$$

due to the unbiasedness and independence of $\mathbf{z}_t$. We can exactly calculate the sum of this geometric series

$$\sum_{j=0}^{T-1}(1-\gamma L)^{2j} = \frac{1-(1-\gamma L)^{2T}}{1-(1-\gamma L)^2} = \frac{1-(1-2\gamma L)^{2T}}{2\gamma L - \gamma^2 L^2} \geq \frac{1}{4\gamma L}$$

where at the last step we used that $\gamma^2 L^2 > 0$ and that $T \geq \frac{\log 2}{\gamma L}$.

And thus the function values are larger than

$$f(\mathbf{x}_T) - f^\star = \frac{L}{2}\left\|\mathbf{x}_T\right\|^2 \geq \frac{L}{2}(1-\gamma L)^{2(t+1)}\left\|\mathbf{x}_0\right\|^2 + \frac{1}{8}\gamma\sigma^2$$

This shows that the noise term in (13) cannot be improved.

E.2. Anti-PGD

This corresponds to Example 3.2. Since $\nabla f(\mathbf{x}) = L\mathbf{x}$, the algorithm (7) for Anti-PGD noise takes a form

$$\begin{aligned}
\mathbf{x}_{t+1} &= (1-\gamma L)\mathbf{x}_t - \gamma\mathbf{z}_{t+1} + \gamma\mathbf{z}_t \\
&= (1-\gamma L)^2\mathbf{x}_{t-1} - (1-\gamma L)\gamma\mathbf{z}_t + (1-\gamma L)\gamma\mathbf{z}_{t-1} - \gamma\mathbf{z}_{t+1} + \gamma\mathbf{z}_t \\
&= (1-\gamma L)^2\mathbf{x}_{t-1} + (1-\gamma L)\gamma\mathbf{z}_{t-1} - \gamma\mathbf{z}_{t+1} + \gamma^2 L\mathbf{z}_t \\
&= (1-\gamma L)^{t+1}\mathbf{x}_0 + (1-\gamma L)^t\gamma\mathbf{z}_1 + \gamma^2 L\sum_{j=1}^{t-1}(1-\gamma L)^{t-j}\mathbf{z}_{j+1} - \gamma\mathbf{z}_{t+1}
\end{aligned}$$

Thus,

$$\begin{aligned}
\mathbb{E}\left\|\mathbf{x}_T\right\|^2 &= (1-\gamma L)^{2T}\left\|\mathbf{x}_0\right\|^2 + (1-\gamma L)^{2(T-1)}\gamma^2\,\mathbb{E}\left\|\mathbf{z}_1\right\|^2 + \gamma^4 L^2\sum_{j=1}^{T-2}(1-\gamma L)^{2(T-1-j)}\,\mathbb{E}\left\|\mathbf{z}_{j+1}\right\|^2 + \gamma^2\,\mathbb{E}\left\|\mathbf{z}_{t+1}\right\|^2 \\
&\geq (1-\gamma L)^{2T}\left\|\mathbf{x}_0\right\|^2 + \gamma^2\sigma^2
\end{aligned}$$

Thus the function values are larger than

$$f(\mathbf{x}_T) - f^\star = \frac{L}{2}\left\|\mathbf{x}_T\right\|^2 \geq (1-\gamma L)^{2T}\left\|\mathbf{x}_0\right\|^2 + \frac{L}{2}\gamma^2\sigma^2$$

This proves that the noise term in (14) cannot be improved.

E.3. Virtual sequence for PGD

In this section we show that for the PGD algorithm, virtual sequences $\tilde{\mathbf{x}}_t$ that are defined in (15) cannot give a tight convergence result.

Since $\tilde{\mathbf{x}}_{t+1} = \tilde{\mathbf{x}}_t - \gamma\nabla f(\mathbf{x}_t)$, and $\nabla f(\mathbf{x}_t) = L\mathbf{x}_t$ we get

$$\tilde{\mathbf{x}}_{t+1} = (1-\gamma L)\tilde{\mathbf{x}}_t + \gamma L(\tilde{\mathbf{x}}_t - \mathbf{x}_t) = (1-\gamma L)\tilde{\mathbf{x}}_t - \gamma^2 L\sum_{j=0}^{t}\mathbf{z}_j$$

where the last equality is since $\tilde{\mathbf{x}}_t - \mathbf{x}_t = -\gamma\sum_{j=1}^{t}\mathbf{z}_j$. Unrolling,

$$\tilde{\mathbf{x}}_{t+1} = (1-\gamma L)\tilde{\mathbf{x}}_t + \gamma L(\tilde{\mathbf{x}}_t - \mathbf{x}_t) = (1-\gamma L)^{t+1}\tilde{\mathbf{x}}_0 - \gamma^2 L\sum_{j=1}^{t}\mathbf{z}_j\sum_{i=0}^{j}(1-\gamma L)^i$$

Thus the norm

$$\mathbb{E}\left\|\tilde{\mathbf{x}}_T\right\|^2 = (1-\gamma L)^{2T}\left\|\mathbf{x}_0\right\|^2 + \gamma^4 L^2\sum_{j=1}^{T-1}\left[\sum_{i=0}^{j}(1-\gamma L)^i\right]^2\sigma^2$$

We can calculate exactly the inner sum as

$$\sum_{i=0}^{j}(1-\gamma L)^i = \frac{1-(1-\gamma L)^j}{\gamma L}$$

and thus

$$\mathbb{E}\left\|\tilde{\mathbf{x}}_T\right\|^2 = (1-\gamma L)^{2T}\left\|\mathbf{x}_0\right\|^2 + \gamma^2\sum_{j=1}^{T-1}\left[1-(1-\gamma L)^j\right]^2\sigma^2 \geq \gamma^2\sum_{j=\frac{T}{2}}^{T-1}\left[1-2(1-\gamma L)^j\right]\sigma^2$$

It is left to note that for T sufficiently large, $T \geq 2\frac{\log 4}{\gamma L}$, it holds that $(1-\gamma L)^{T/2} \leq \frac{1}{4}$ and thus $\left[1-2(1-\gamma L)^j\right] \geq \frac{1}{2}$. Using this, we arrive

$$\mathbb{E}\left\|\tilde{\mathbf{x}}_T\right\|^2 \geq \gamma^2\sigma^2\frac{T}{4}$$

and this the function value $f(\tilde{\mathbf{x}}_T) \geq L\gamma^2\sigma^2\frac{T}{8}$.